S-Crescendo: A Nested Transformer Weaving Framework for Scalable Nonlinear System in S-Domain Representation

Junlang Huang[1,*], Hao Chen[1,*], Li Luo[1,†], Yong Cai[1,†], Lexin Zhang[1], Tianhao Ma[1], Yitian Zhang[1],
Zhong Guan[1,✉]

Abstract

Simulation of high-order nonlinear system requires extensive computational resources, especially in modern VLSI backend design where bifurcation-induced instability and chaos-like transient behaviors pose challenges. We present S-Crescendo - a nested transformer weaving framework that synergizes S-domain with neural operators for scalable time-domain prediction in high-order nonlinear networks, alleviating the computational bottlenecks of conventional solvers via Newton-Raphson method. By leveraging the partial-fraction decomposition of an n-th order transfer function into first-order modal terms with repeated poles and residues, our method bypasses the conventional Jacobian matrix-based iterations and efficiently reduces computational complexity from cubic $O(n^3)$ to linear $O(n)$.The proposed architecture seamlessly integrates an S-domain encoder with an attention-based correction operator to simultaneously isolate dominant response and adaptively capture higher-order non-linearities. Validated on order-1 to order-10 networks, our method achieves up to 0.99 test-set R^2 accuracy against HSPICE golden waveforms and accelerates simulation by up to 18×, providing a scalable, physics-aware framework for high-dimensional nonlinear modeling.

1 Introduction

In recent years, deep learning technologies have made remarkable progress, with Transformer-based architectures demonstrating exceptional performance and significant advantages in fields such as natural language processing (NLP), computer vision, and time-series data modeling.[1] Transformer models, by effectively capturing complex relationships and long-range dependencies, offer a novel perspective for data-driven modeling. This technological advancement has inspired researchers to explore its potential applications in traditional engineering domains, especially in complex physical modeling and signal prediction[2][3].

Nonlinear system identification remains a core challenge across many domains, particularly under high-order dynamics, non-stationarity, and limited observability. Classical methods from control theorysuch as Volterra series, HammersteinWiener models, and grey-box approachestypically decompose system behavior into a linear core and a nonlinear correction [4, 5, 6, 7]. However, their scalability and generalization degrade in high-dimensional parameter spaces [8]. These limitations are especially pronounced in modern integrated circuit design, where nonlinearities emerge not only from active devices but also from parasitic effects in passive interconnects. A canonical example is the "nonlinear driver + linear RC load" configuration, illustrated in Figure 1. As technology scales, interconnect parasitics exhibit strong dynamic nonlinearities due to proximity effects, process variation, and material inhomogeneity [9], complicating accurate modeling. To address this, we propose a neural operator framework that integrates Laplace-domain physical priors with data-driven adaptability. Demonstrated on RC current response tasks, this method extends naturally to

39th Conference on Neural Information Processing Systems (NeurIPS 2025).

systems governed by partial differential equations with nonlinear boundary conditions, offering a scalable and physically consistent approach to complex system identification.

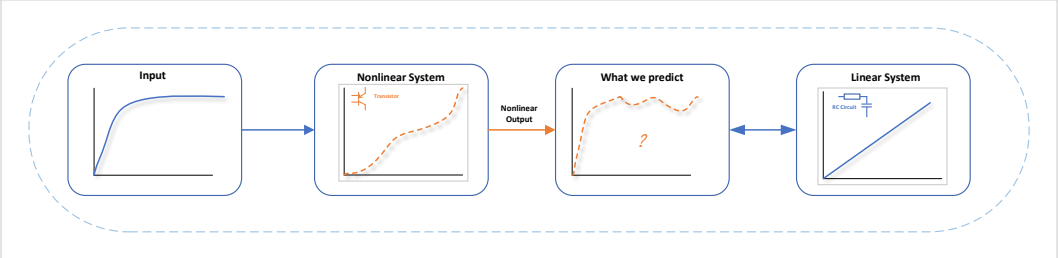

Figure 1: Given a known input signal, the task is to predict the nonlinear systems output before it feeds into the linear system. This intermediate signal, marked in red, is unknown and serves as the prediction target of our model.

In response, a growing body of research has applied deep learning to nonlinear system identification. Approaches based on recurrent networks[10], attention mechanisms[11], and neural operators[12] (e.g., DeepONet[13], FNO[14], and PINNs) have shown promise, particularly in low-dimensional settings or for PDE systems with known boundary conditions. Yet, these methods often require large datasets, lack robustness to structural variation, and suffer from poor physical interpretability[15][16]. More critically, few methods explicitly leverage the modal structure or transfer function representation intrinsic to many engineered systems. As a result, they remain constrained by either computational inefficiency (due to iterative solvers like Newton–Raphson) or limited generalization to systems with unseen topologies or higher-order dynamics[17][15][18][19].While deep learning has been explored for general system identification, its application to signal-line RC response modelinga canonical high-order nonlinear problemremains largely unexplored. Most existing methods still fall under three classical paradigms: Current Source Models (CSMs) [20, 21], Voltage Response Models (VRMs) [22], and Direct Waveform Prediction [23]. Each faces practical limitations: CSMs lack waveform fidelity due to fixed capacitance abstraction [24], VRMs suffer from high cost and solver-induced errors [25, 26], and direct fitting fails under sharp transitions due to overshoot and undershoot distortion.

Against this backdrop, Transformer-based methods offer a powerful new tool for nonlinear system identification in the S-domain. Transformer architectures excel at capturing complex, long-range dependencies and higher-order interactions, making them ideally suited to address the limitations of traditional RC-network models in time-domain response prediction [1].

Even in nominally high-order interconnects, only a handful of dominant poles govern signal behavior. Standard model order reduction (MOR) selects these modes, typically fewer than ten by energy or gain thresholds, and collapses a 5000th order RC network into a low-order surrogate with minimal frequency response error [27, 28]. Going beyond linear reduction, we encode each reduced first-order term into a learned latent embedding and apply an attention-driven correction operator to capture nonlinear driver-load effects. On 4th to 10th order surrogates, our method attains R^2 up to 0.99 against HSPICE waveforms, evidencing superior accuracy. By leveraging partial-fraction decomposition, we decouple topology from prediction-forecasting each modal response independently in the S-domain before summation, thus ensuring universality and structural agnosticism.We introduce a physics awared S-domain neural operator that seamlessly integrates with MOR pipelines, delivering a scalable, accurate, and efficient solution for nonlinear RC simulation, electromagnetic analysis, and signal-integrity evaluation without fixed driver or load models.

The proposed model adopts a two-stage architecture: a base module first predicts individual first-order responses from partial fraction decomposition and aggregates them into a baseline output. A subsequent compensation network then iteratively refines this output by learning residual corrections across model orders. This overall architecture is illustrated in Figure 2.

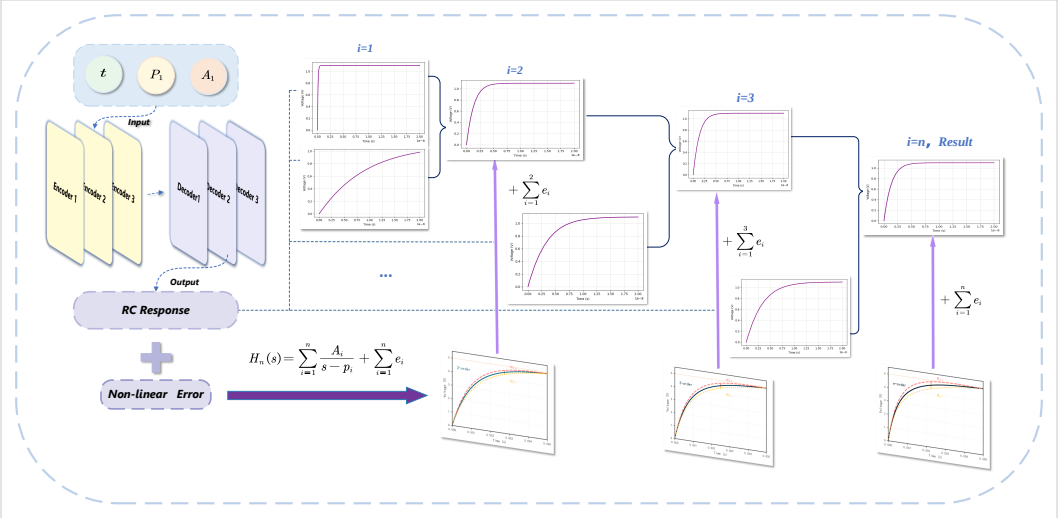

Figure 2: **Model Overview.** The model first constructs a baseline prediction by summing the first-order responses of pole-residue pairs. For each mode i, the residual module e_i is trained using the current and previous poles, residues, and time information to correct the accumulated error. Residuals are added iteratively to refine the final prediction.

2 Theoretical Background

2.1 *Decomposition Theorem for High-Order RC Network Transfer Functions*

Modeling nonlinear dynamical systems remains fundamental across many physical domains, where complex interactions often overlay intrinsic linear behaviors. In integrated circuit design, a prominent instance arises in interconnects, where nonlinear drivers interface with passive metal wires forming linear time-invariant (LTI) networks. The passive portion, shaped by parasitic resistances (R_i) and capacitances (C_i), governs signal delay, attenuation, and waveform distortion. The behavior of these RC networks is typically characterized in the Laplace domain via a transfer function $H(s)$ that maps input signals to output responses [27, 29, 4]. For a network with m independent energy-storage elements, the transfer function takes the form shown in Equation (1):

$$H(s) = \frac{N(s)}{D(s)} = \frac{b_0 + b_1 s + \cdots + b_{m-1} s^{m-1}}{a_0 + a_1 s + \cdots + a_m s^m}. \tag{1}$$

where the roots of the denominator $D(s)$ are the system poles $p_i = -1/\tau_i = -1/(R_i C_i)$, all located on the negative real axis due to the passive nature of RC circuits.

By the fundamental theorem of algebra and the Heine-Borel theorem, any strictly proper rational function with distinct poles admits a unique partial fraction expansion[30] shown in Equation (2):

$$H(s) = \sum_{i=1}^{m} \frac{r_i}{s - p_i}, \quad r_i = \left. \frac{N(s)}{D'(s)} \right|_{s=p_i}. \tag{2}$$

This decomposition can be rigorously derived through two classical approaches. First, the method of undetermined coefficients constructs a linear system whose solution is guaranteed by the nonsingularity of the associated Vandermonde matrix when all poles are distinct. Second, the Cauchy residue theorem establishes the residue-based representation by integrating $H(s)$ around a closed contour enclosing all poles; analytic continuation then ensures the uniqueness of this expansion.

Further physical constraints arise from the realizability conditions of RC networks. All poles must lie strictly in the negative real domain to ensure overdamped and stable dynamics. While residues are typically real-valued, they may be either positive or negative, reflecting modal interference effects in higher-order coupled systems. Despite potential non-monotonicity at the modal level, the overall response remains physically consistent and interpretable, capturing the multi-timescale nature of signal propagation inherent to real interconnect behavior.

2.2 *Generalization to Repeated Poles*

When a pole p_i of the transfer function has multiplicity $k_i > 1$ (with $\sum_i k_i = m$), the partial-fraction expansion naturally extends to form in Equation (3):

$$H(s) = \sum_{i=1}^{q} \sum_{j=1}^{k_i} \frac{r_{ij}}{(s - p_i)^j}, \tag{3}$$

where each higher-order residue is given by Equation (4):

$$r_{ij} = \frac{1}{(k_i - j)!} \frac{d^{k_i - j}}{ds^{k_i - j}} \left[(s - p_i)^{k_i} H(s) \right] \Big|_{s = p_i}. \tag{4}$$

In practice, however, exact repeated poles are rare in on-chip RC networks due to manufacturing tolerances and layout variations. Even when poles are nearly coincident, the corresponding higher-order residues r_{ij} tend to be small, and their time domain contributions $t^{j-1} e^{p_i t}$ decay rapidly for $p_i < 0$. Consequently, one can safely ignore repeated-pole terms in most modeling tasks and rely on single-pole expansions to achieve high-fidelity simulations [31].

This comprehensive decomposition provides a unified framework for both time-domain and frequency-domain analysis of arbitrary high-order RC interconnect networks.

2.3 Computational Complexity Analysis

Traditional SPICE-based transient simulation begins by formulating a system of nonlinear equations based on circuit devices and Kirchhoffs laws. Solving this systemtypically via the NewtonRaphson methodis computationally expensive. For an n-node RC network, each iteration involves Jacobian construction and LU decomposition, resulting in a complexity of $\mathcal{O}(n^3)$. Even with sparse solvers, fill-in effects lead to an effective cost between $\mathcal{O}(n^{2.5})$ and $\mathcal{O}(n^3)$ over T time steps and P ports [32, 33].

In contrast, our method operates in the S-domain and eliminates matrix inversion. Computing the admittance or impedance to a single output node requires $\mathcal{O}(n)$ operations. Extending this to all n nodes yields a total complexity of $\mathcal{O}(n^2)$, while avoiding iterative linear system solves.

3 Data Acquisition and Preprocessing

3.1 Simulation Environment Setup

The HSPICE simulation platform employing a 40-nm CMOS PDK ensured process-compliant device parameters (V_{th}, λ, I_{leak}), where a single-stage CMOS driver with IEEE 1481-2009-compliant RC networks (parasitics extracted via Python) was modeled through state space representation and converted to an S-domain transfer function; subsequent partial fraction decomposition yielded first-order subsystems characterized by poles p_i and residues r_i for neural operator-based time domain prediction.

3.2 Stimulation Configuration

The input voltage waveform was configured as an ideal step signal (0 to VDD transition). Transient simulations covered both the signal rise phases (0 to 20 ns) and steady state behavior,with a time step resolution of 10ps.

3.3 Feature Representation and Supervision

Each sample is defined by a tuple of conditioning inputs and supervised outputs. The conditioning inputs comprise a device type label, a sequence of transient time points $t_1, \ldots, t_T$, and a set of frequency domain features obtained via transfer function decomposition, encoded as poleresidue pairs $\{(p_i, r_i)\}_{i=1}^{m}$. Together, these inputs capture the structural, temporal, and modal characteristics of the circuit.

The supervised target is the voltage response sequence $\{V_{\text{out}}(t_1), \ldots, V_{\text{out}}(t_T)\}$, obtained from HSPICE simulation, which guides training via time-aligned regression.

3.4 Feature Normalization

To harmonize heterogeneous input features and enhance model robustness, we apply the following transformations in a single step shown in Equation (5):

$$V'(t) = \frac{V(t) - \min(V)}{\max(V) - \min(V)}, \qquad t' = \frac{\log_{10}(t) - \mu_t}{\sigma_t} \tag{5}$$

where $V(t)$ is the original voltage at time t, $\min(V)$ and $\max(V)$ are its minimum and maximum over the waveform, t is a sampled transient time point, and μ_t, σ_t are the mean and standard deviation of $\log_{10}(t)$ across all samples. These normalizations place both features on comparable scales, mitigate the influence of outliers, and promote stable, efficient training.

3.5 Transfer Function-Based RC Network Modeling

We propose a compact, system-level modeling framework for standard-cell-driven RC interconnects by decomposing the Laplace-domain transfer function shown in Equation (6):

$$H(s) = \frac{V_{\text{out}}(s)}{V_{\text{in}}(s)} == \sum_{i=1}^{n} \frac{A_i}{\frac{s}{p_i} - 1} \tag{6}$$

where each decay rate $p_i > 0$ (inverse time constant) and residue $A_i \in \mathbb{R}$ satisfies $\sum_i A_i = 1$, ensuring a normalized unit-step response. This form captures the dominant exponential kernels $e^{-p_i t}$ without explicit node-level modeling.

To enable neuralnetwork learning and generalization across circuits of varying size, we encode each mode as a pole-residue pair (p_i, A_i), normalize all p_i and A_i by $\max_i p_i$ and $\max_i |A_i|$, sort pairs by descending $|A_i|$. This interpretable mode sequence accurately reconstructs high-order RC responses with linear complexity and full spectral fidelity.

4 Model Architecture Design

4.1 Baseline Module: First-Order Prediction

The baseline module predicts the nonlinear voltage response of a single-mode RC system, specified by a pole-residue pair (p, r), at discrete time points $\{t_k\}_{k=1}^{T}$. Unlike ideal linear RC networks, the input waveform here first passes through nonlinear active components (e.g., CMOS drivers), making the overall system response analytically intractable. To address this, we employ a neural function approximator:$\hat{V}(t_k) = f_\theta(p, r, t_k)$.where f_θ is a lightweight Transformer trained to capture the nonlinear mapping from modal and temporal inputs to voltage outputs[1].

The model consists of three encoder and three decoder layers, each composed of multi-head self-attention, feed-forward sublayers with GELU activation, and layer normalization[34]. Positional encoding is included to preserve temporal structure. Input features (p, r, t_k) are embedded and processed in parallel to predict $\hat{V}(t_k)$ at each time step. The network is trained end-to-end using the AdamW optimizer with weight decay, minimizing the mean squared error[35][36] shown in Equation (7):

$$\mathcal{L}_{\text{MSE}} = \frac{1}{T} \sum_{k=1}^{T} \big(\hat{V}(t_k) - V(t_k)\big)^2 \tag{7}$$

This architecture provides an accurate and generalizable first-order predictor that forms the foundation for modeling higher-order RC systems through residual correction.

4.2 Compensation Module: Residual Correction

The compensation module iteratively refines the baseline prediction by learning the residual error between successive model orders. For each order n and time point t_k, the input feature vector is $\big(n,\ p_n,\ r_n,\ p_{n-1},\ r_{n-1},\ t_k\big)$.where (p_n, r_n) and (p_{n-1}, r_{n-1}) denote the pole-residue pairs for the nth and $(n-1)$th modes, respectively.The network outputs shown in Equation (8):

$$\hat{e}_n(t_k) = g_\phi\big(n, p_n, r_n, p_{n-1}, r_{n-1}, t_k\big) \tag{8}$$

which represents the corrective residual to be added to the order-n prediction at time t_k.

The function g_ϕ is implemented as a lightweight Transformer with the same depth and hyperparameters as the baseline module. It is trained end-to-end using the AdamW optimizer to minimize the residual mean squared error, thereby progressively correcting and refining higher-order predictions.

4.3 Recursive Training Procedure

Let $\{(p_i, r_i)\}_{i=1}^{n}$ be the pole-residue pairs for the nth-order model and $\{t_k\}_{k=1}^{T}$ the sampled time points. Denote by f_θ the trained first-order predictor and by $\{e_{\phi_j}\}_{j=1}^{n-1}$ the sequence of learned residual modules up to order $n-1$. To train the nth residual module e_{ϕ_n}, we first accumulate the baseline prediction by summing $f_\theta(p_i, r_i, t_k)$ for $i = 1, \ldots, n$. We then add all previously learned corrections e_{ϕ_j} to form the current prediction and compute its discrepancy from the true output $V_{\text{out}}(t_k)$. This residual error serves as the target for e_{ϕ_n}, which is fit by minimizing the mean squared error over $k = 1, \ldots, T$ using the AdamW optimizer. Repeating this process for each order yields a cascade of lightweight modules that progressively refine the high-order RC response.

Algorithm 1 Iterative Residual Correction Training

Require: Base predictor f_θ, residual module set $\{e_{\phi_j}\}_{j=1}^{N}$, sampled data $\{t_k, V_{\text{out}}(t_k)\}_{k=1}^{T}$
Ensure: Trained residual modules $\{e_{\phi_j}\}_{j=1}^{N}$

Initialize cumulative baseline prediction: $\hat{V}_{\text{base}}(t_k) \leftarrow 0,\ \forall k \in [1, T]$
for residual index $j = 1$ **to** N **do**
    Load current pole p_j and residue r_j
Phase 1: Baseline prediction update
    for time step $k = 1$ **to** T **do**
        Update baseline: $\hat{V}_{\text{base}}(t_k) \leftarrow \hat{V}_{\text{base}}(t_k) + f_\theta(p_j, r_j, t_k)$
    end for
Phase 2: Residual target computation
    for time step $k = 1$ **to** T **do**
        Compute current prediction:

$$\hat{V}_j(t_k) \leftarrow \hat{V}_{\text{base}}(t_k) + \sum_{i=1}^{j-1} e_{\phi_i}(i, p_i, r_i, p_{i-1}, r_{i-1}, t_k)$$

        Compute residual target:

$$r_j(t_k) \leftarrow V_{\text{out}}(t_k) - \hat{V}_j(t_k)$$

    end for
Phase 3: Module training
    Build training set: $\mathcal{D}_j = \{(t_k, r_j(t_k))\}_{k=1}^{T}$
    Minimize the loss:

$$\min_{\phi_j} \frac{1}{T} \sum_{k=1}^{T} \big(e_{\phi_j}(j, p_j, r_j, p_{j-1}, r_{j-1}, t_k) - r_j(t_k)\big)^2$$

    Update ϕ_j using gradient descent
end for

By repeating this procedure for $n = 1, 2, \ldots, N$, we ensure each e_{ϕ_n} learns to generalize the correction from order $n-1$ to n, yielding a cascade of residual models that together approximate the full highorder response with minimal overfitting.Moreover, this recursive training scheme offers a degree of generalization. Each residual module e_{ϕ_n} depends only on the poleresidue pairs of two adjacent orders and the current time point, without requiring knowledge of the full network topol-

ogy or total number of nodes. As a result, the trained modules can be reasonably extended to refine predictions for moderately higher-order systems beyond those seen during training.

4.4 Inference Procedure

In the inference stage, we compute a single forward-pass estimate of the output waveform by first assembling a baseline response and then applying all residual corrections in parallel. Specifically, for each time sample t_k shown in Equation (9):

$$\hat{V}_{\text{base}}(t_k) = \sum_{i=1}^{N} f_\theta(p_i, r_i, t_k) \tag{9}$$

where p_i is the ith pole (inverse time constant) of the transfer function, r_i is the corresponding residue (modal weight), and $f_\theta(p_i, r_i, t_k)$ denotes the base predictors output, typically $r_i e^{-p_i t_k}$.

All N residual modules e_{ϕ_j} are then evaluated and summed in parallel shown in Equation (10):

$$\hat{V}_N(t_k) = \hat{V}_{\text{base}}(t_k) + \sum_{j=1}^{N} e_{\phi_j}\left(j, p_j, r_j, p_{j-1}, r_{j-1}, t_k\right) \tag{10}$$

where $e_{\phi_j}(\cdot)$ is the jth trained residual correction module, and its inputs $(j, p_j, r_j, p_{j-1}, r_{j-1}, t_k)$ include the current and previous pole-residue pairs as well as the time t_k.

This procedure yields the final prediction $\hat{V}_N(t_k)$ at each t_k with $\mathcal{O}(N)$ complexity, running 5–10$\times$ faster than commercial tools like HSPICE by requiring just a single pass through the base predictor and residual modules.

5 Experiment

5.1 SinglePole Transfer Function: Training and Test Performance

We first evaluate the performance of our model on singlepole transfer functions. The model achieves nearperfect fit on the training data and strong generalization to unseen singlepole functions.

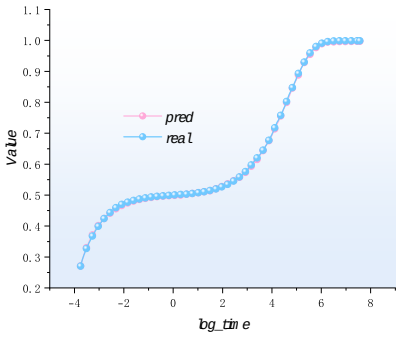

(a) Single-Pole Transfer Function: Training vs. test performance. $R^2 = 0.999$ illustrates near-perfect fit on the training data and strong generalization on held-out single-pole examples.

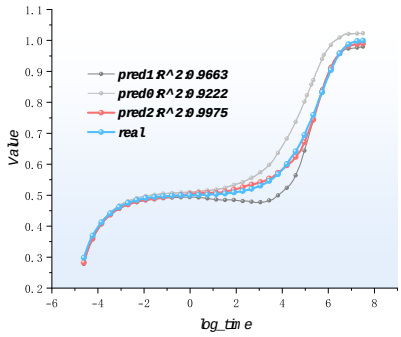

(b) Error-Correction Model: This figure illustrates the step-by-step waveform correction process, from the raw prediction without any error correction through the successive application of first, second, and third-order error modules, culminating in a final fit of $R^2 = 0.9975$

Figure 3: (a) Model performance on single-pole transfer functions, showing minimal overfitting and excellent test-set accuracy. (b) Effectiveness of our recursive error-correction module on a three-pole example.

5.2 Effectiveness of the Error-Correction Model

To demonstrate the benefit of our recursive error-correction module, we evaluate on a three-pole transfer function example shown in Equation (11):

$$H(s) = \sum_{i=1}^{3} \frac{A_i}{\frac{s}{p_i} - 1} \tag{11}$$

where $\{p_i\}$ and $\{A_i\}$ are chosen such that the poles are well separated. Figure 3 shows the predicted and true step responses over time. We compute the coefficient of determination and obtain $R^2 = 0.9975$, confirming that the error-correction stage significantly improves accuracy over the base model.

5.3 Generalization to Higher-Order Transfer Functions

Next, we evaluate the models ability to generalize beyond training orders. We train exclusively on systems of order within 3 and then evaluate on transfer functions of orders from 4 to 9. Table 1 reports MSE and R^2 on each higher-order test set. Despite never having seen orders above 3, the model retains strong predictive power, demonstrating effective extrapolation. To probe more extreme extrapolation, we additionally train an error-correction model on 15th-order systems and test it on 200th-order transfer functions; the full setup and per-case results are provided in the appendix. Across 20 held-out cases, the mean R^2 reaches 0.983 (see Appendix).

Order	4	5	6	7	8	9
R^2	0.986	0.997	0.995	0.990	0.979	0.964

Table 1: Generalization performance on higher-order transfer functions (trained on orders ≤ 3).

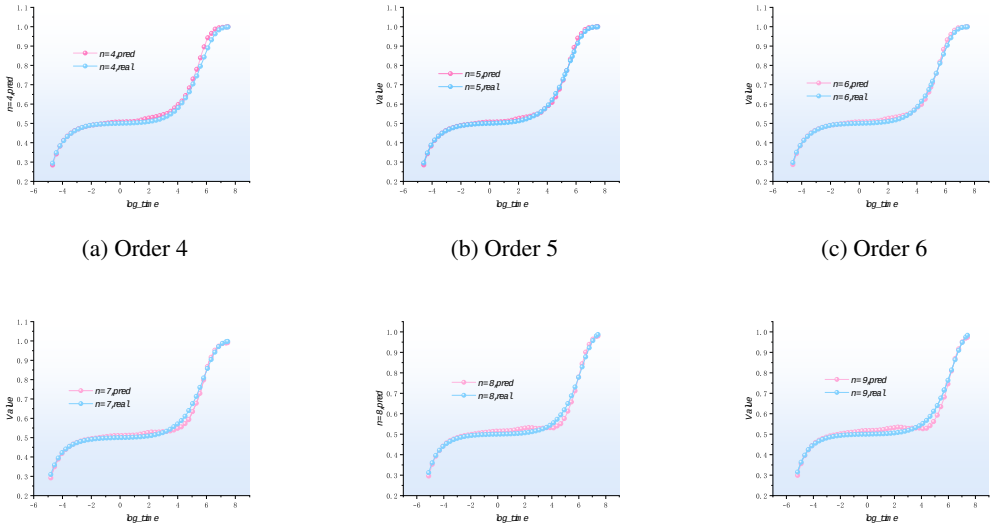

(a) Order 4 (b) Order 5 (c) Order 6

(d) Order 7 (e) Order 8 (f) Order 9

Figure 4: Prediction vs. true response for transferfunction orders 4 to 9.

5.4 Inference Time Comparison

Training cost. Each residual-correction module contains approximately 100K160K parameters. All models were trained on a single NVIDIA RTX 4090 GPU. For reference, single-pole systems typically train in under 20 minutes, while 10th-order systems converge in approximately 2 hours. Given the considerable acceleration our model achieves at inference time, this one-time training cost is highly acceptable.

Dataset construction. Training data is generated using standard *HSPICE* simulations. Each simulation typically completes in about 0.5 seconds. For our full training dataset of $\sim 5{,}000$ samples,

the end-to-end preprocessing pipeline (simulation, waveform extraction, and supervised data formatting) completes in under 2 hours. The process is fully scriptable and parallelizable, and does not pose a practical bottleneck.

Runtime comparison. Finally, we compare the runtime of our S-Crescendo model against *HSPICE* on a 10 ns transient simulation sampled at 1,000 time steps. *HSPICE* runtimes for orders 1 through 10 were measured on a CPU node equipped with an AMD EPYC 7763 (64 cores) and 256 GB of DDR4 RAM; S-Crescendo inference times were recorded on a workstation with an NVIDIA RTX 4090 GPU. Table 2 reports the average simulation and inference times. Across all orders, S-Crescendo achieves more than two orders of magnitude speedup while preserving high accuracy.

DCM baseline. Dynamic Circuit Macromodeling (DCM) is a physics-inspired model-order reduction technique that constructs dynamic macromodels to balance accuracy and efficiency. On the same 10-order RC test file, DCM completes in 0.6 s with a fit accuracy of $R^2 = 0.9983$.[1]

NGSPICE baseline. *NGSPICE* is a widely used open-source SPICE simulator adopted across academia and industry. Although typically slower than commercial tools such as *HSPICE*, its accessibility and device-level accuracy make it a credible practical reference. On our 10-order RC test file, *NGSPICE* completes in 1.08 s andbecause it shares core numerical algorithms with *HSPICE*delivers equivalently high fidelity (we did not compute a separate R^2 against *HSPICE*).[2]

Note. Order-10 is the *slowest* inference case for our model; benchmarking against this conservative worst case still yields the above margins over DCM, NGSPICE, and HSPICE, underscoring the strength of our approach.

Table 2: Runtime comparison between HSPICE and S-Crescendo across transfer function orders (10ns, 1000 steps).

Order	1	2	3	4	5	6	7	8	9	10
HSPICE (s)	0.26	0.21	0.23	0.22	0.27	0.26	0.28	0.23	0.23	0.26
S-Crescendo (s)	0.014	0.019	0.022	0.018	0.023	0.028	0.031	0.034	0.039	0.042
Speedup (X)	18.6	11.1	10.5	12.2	11.7	9.3	9.0	6.8	5.9	6.2

6 Further Discussion

6.1 Degradation of Accuracy at Higher Orders

While S-Crescendo performs well on low to mid-order transfer functions, its R^2 degrades as order m increases. This is due to recursive error accumulation: each correction module $\varepsilon_k(t)$ adjusts not only current residuals but also propagates previous errors. If the single-pole state space has size N, then the full m-pole space grows as N^m, whereas each error model sees only N samples during training. Thus, the fraction of covered states is shown in Equation (12):

$$\frac{N \times m}{N^m} \tag{12}$$

which shrinks rapidly with m, leading to sparse supervision and compounded inaccuracies.

6.2 Reducing Data Dependency via Blocked Recursion

To alleviate error accumulation and data explosion, we propose a blocked recursion strategy. Instead of training a separate module per order, we group adjacent orders into blocksfor example, a shared module for orders 24, another for 56, etc. Each block is supervised on $O(N \times B)$ states (for block size B), yet extrapolates across B orders. This reduces the number of recursive calls and lowers training demands, improving both runtime and scalability.

[1] All DCM runtimes were measured on a machine with AMD EPYC 7763 (64 cores), 1 TB RAM, and 30 GB swap.

[2] NGSPICE runtime was measured on a machine with Intel Core i7-14650HX CPU and 32 GB RAM. S-Crescendo inference uses the same RTX 4090 workstation described in this paper.

6.3 Scaling of Inference Latency with Order

S-Crescendo's inference latency scales roughly linearly with order m, since each pole adds a forward pass. In contrast, tools like HSPICE collapse high-order dynamics via model reduction, maintaining near-constant runtime. To bridge this gap, we consider (i) collapsing low-impact poles into aggregate corrections, or (ii) integrating model-order reduction into the learned pipelineboth strategies aim to extend our efficiency gains to large-scale systems.

6.4 Modeling Limitation: Repeated Poles in Transfer Functions

The model currently does not handle repeated poles, which introduce higher-order temporal terms like $t^k e^{\lambda t}$. To address this, future models can extend input features to include pole multiplicity, enabling learning from triplets (p_i, A_i, m_i). This would broaden the model's applicability to more complex, higher-order dynamics.

6.5 Outlook: Toward General NonlinearLinear Hybrid Systems

Beyond RC modeling, the proposed framework extends naturally to hybrid systems with a "nonlinear front-end + linear dynamic core" architecture, common across engineering domains. Examples include switching converters in power electronics, where nonlinear control drives linear filters; analog front-ends, where transistor drivers interface with RC loads; and neural membrane models coupling nonlinear ion channels to capacitive elements. By modeling linear dynamics via Laplace-domain priors and learning nonlinear corrections, the framework enables efficient, interpretable emulation. Future directions include integrating operator learning or domain-specific constraints to broaden applicability.

7 Acknowledgments and Disclosure of Funding

This work was supported by the National Natural Science Foundation of China (NSFC) under Grant 62374189.

References

[1] Ashish Vaswani, Noam Shazeer, Niki Parmar, Jakob Uszkoreit, Llion Jones, Aidan N Gomez, Łukasz Kaiser, and Illia Polosukhin. Attention is all you need. *Advances in neural information processing systems*, 30, 2017.

[2] Jacob Devlin, Ming-Wei Chang, Kenton Lee, and Kristina Toutanova. Bert: Pre-training of deep bidirectional transformers for language understanding. In *Proceedings of the 2019 conference of the North American chapter of the association for computational linguistics: human language technologies, volume 1 (long and short papers)*, pages 4171–4186, 2019.

[3] Johannes Schneider and Michalis Vlachos. A survey of deep learning: From activations to transformers. *arXiv preprint arXiv:2302.00722*, 2023.

[4] Athanasios C Antoulas. *Approximation of large-scale dynamical systems*. SIAM, 2005.

[5] Zhaohui Cen, Jiaolong Wei, and Rui Jiang. A grey-box neural network based identification model for nonlinear dynamic systems. In *The Fourth International Workshop on Advanced Computational Intelligence*, pages 300–307. IEEE, 2011.

[6] Martin Schetzen. Nonlinear system modeling based on the wiener theory. *Proceedings of the IEEE*, 69(12):1557–1573, 1981.

[7] Adrian Wills, Thomas B Schön, Lennart Ljung, and Brett Ninness. Identification of hammerstein–wiener models. *Automatica*, 49(1):70–81, 2013.

[8] Johan Schoukens and Lennart Ljung. Nonlinear system identification: A user-oriented road map. *IEEE Control Systems Magazine*, 39(6):28–99, 2019.

[9] Devendra Kumar Sharma, BK Kaushik, and RK Sharma. Vlsi interconnects and their testing: prospects and challenges ahead. *Journal of Engineering, Design and Technology*, 9(1):63–84, 2011.

[10] Max Schüssler, Tobias Münker, and Oliver Nelles. Deep recurrent neural networks for nonlinear system identification. In *2019 IEEE symposium series on computational intelligence (SSCI)*, pages 448–454. IEEE, 2019.

[11] Maziar Raissi, Paris Perdikaris, and George E Karniadakis. Physics-informed neural networks: A deep learning framework for solving forward and inverse problems involving nonlinear partial differential equations. *Journal of Computational physics*, 378:686–707, 2019.

[12] Ricky TQ Chen, Yulia Rubanova, Jesse Bettencourt, and David K Duvenaud. Neural ordinary differential equations. *Advances in neural information processing systems*, 31, 2018.

[13] Lu Lu, Pengzhan Jin, Guofei Pang, Zhongqiang Zhang, and George Em Karniadakis. Learning nonlinear operators via deeponet based on the universal approximation theorem of operators. *Nature machine intelligence*, 3(3):218–229, 2021.

[14] Zongyi Li, Nikola Kovachki, Kamyar Azizzadenesheli, Burigede Liu, Kaushik Bhattacharya, Andrew Stuart, and Anima Anandkumar. Fourier neural operator for parametric partial differential equations. *arXiv preprint arXiv:2010.08895*, 2020.

[15] Erlend Torje Berg Lundby, Adil Rasheed, Ivar Johan Halvorsen, Dirk Reinhardt, Sebastien Gros, and Jan Tommy Gravdahl. Deep active learning for nonlinear system identification. *arXiv preprint arXiv:2302.12667*, 2023.

[16] Gianluigi Pillonetto, Aleksandr Aravkin, Daniel Gedon, Lennart Ljung, Antônio H Ribeiro, and Thomas B Schön. Deep networks for system identification: a survey. *Automatica*, 171: 111907, 2025.

[17] Max Revay, Ruigang Wang, and Ian R Manchester. Recurrent equilibrium networks: Flexible dynamic models with guaranteed stability and robustness. *IEEE Transactions on Automatic Control*, 69(5):2855–2870, 2023.

[18] Carl Andersson, Antônio H Ribeiro, Koen Tiels, Niklas Wahlström, and Thomas B Schön. Deep convolutional networks in system identification. In *2019 IEEE 58th conference on decision and control (CDC)*, pages 3670–3676. IEEE, 2019.

[19] Kaicheng Niu, Mi Zhou, Chaouki T Abdallah, and Mohammad Hayajneh. Deep transfer learning for system identification using long short-term memory neural networks. *arXiv preprint arXiv:2204.03125*, 2022.

[20] John F Croix and DF Wong. Blade and razor: cell and interconnect delay analysis using current-based models. In *Proceedings of the 40th annual Design Automation Conference*, pages 386–389, 2003.

[21] Synopsys. Composite current source (ccs). Online. URL http://www.opensourceliberty.org/ccspaper. Accessed: 2025-03-29.

[22] Jessica Qian, Satyamurthy Pullela, and Lawrence Pillage. Modeling the" effective capacitance" for the rc interconnect of cmos gates. *IEEE Transactions on Computer-Aided Design of Integrated Circuits and Systems*, 13(12):1526–1535, 1994.

[23] Palkesh Jain and Ankit Jain. Accurate current estimation for interconnect reliability analysis. *IEEE Transactions on very large scale Integration (VLSI) Systems*, 20(9):1634–1644, 2011.

[24] Chirayu Amin, Chandramouli Kashyap, Noel Menezes, Kip Killpack, and Eli Chiprout. A multi-port current source model for multiple-input switching effects in cmos library cells. In *Proceedings of the 43rd annual Design Automation Conference*, pages 247–252, 2006.

[25] Soroush Abbaspour and Massoud Pedram. Calculating the effective capacitance for the rc interconnect in vdsm technologies. In *Proceedings of the 2003 Asia and South Pacific Design Automation Conference*, pages 43–48, 2003.

[26] Minglu Jiang, Qiang Li, Zhangcai Huang, and Yasuaki Inoue. A non-iterative effective capacitance model for cmos gate delay computing. In *2010 International Conference on Communications, Circuits and Systems (ICCCAS)*, pages 896–900. IEEE, 2010.

[27] Altan Odabasioglu, Mustafa Celik, and Lawrence T Pileggi. *PRIMA: Passive reduced-order interconnect macromodeling algorithm*. Springer, 2003.

[28] Kang Cheng, Zuochang Ye, and Wenjian Yu. Model order reduction for large scale rc networks based on optimal elimination. *Journal of Computer-Aided Design & Computer Graphics*, 24 (11):1506–1512, 2012.

[29] Peter Feldmann and Roland W Freund. Efficient linear circuit analysis by padé approximation via the lanczos process. *IEEE Transactions on Computer-Aided Design of Integrated Circuits and Systems*, 14(5):639–649, 2002.

[30] Katsuhiko Ogata et al. *Modern control engineering*. Prentice Hall India, 2009.

[31] Bernard N Sheehan. Realizable reduction of rc networks. *IEEE Transactions on Computer-Aided Design of Integrated Circuits and Systems*, 26(8):1393–1407, 2007.

[32] Timothy A Davis. *Direct methods for sparse linear systems*. SIAM, 2006.

[33] James W Demmel. *Applied numerical linear algebra*. SIAM, 1997.

[34] Dan Hendrycks and Kevin Gimpel. Gaussian error linear units (gelus). *arXiv preprint arXiv:1606.08415*, 2016.

[35] Ilya Loshchilov and Frank Hutter. Decoupled weight decay regularization. *arXiv preprint arXiv:1711.05101*, 2017.

[36] Yoshua Bengio, Ian Goodfellow, Aaron Courville, et al. *Deep learning*, volume 1. MIT press Cambridge, MA, USA, 2017.

[37] Ph Lindorfer and C Bulucea. Modeling of vlsi mosfet characteristics using neural networks. In *Simulation of Semiconductor Devices and Processes: Vol. 5*, pages 33–36. Springer, 1993.

[38] Palanisamy Kalpana and Kandasamy Gunavathi. Test-generation-based fault detection in analog vlsi circuits using neural networks. *ETRI journal*, 31(2):209–214, 2009.

[39] Xiaolei Ding, Vijay K Devabhaktuni, Biswarup Chattaraj, Mustapha CE Yagoub, Makarand Deo, Jianjun Xu, and Qi Jun Zhang. Neural-network approaches to electromagnetic-based modeling of passive components and their applications to high-frequency and high-speed nonlinear circuit optimization. *IEEE Transactions on Microwave Theory and Techniques*, 52(1): 436–449, 2004.

[40] Igor Keller, Ken Tseng, and Nisath Verghese. A robust cell-level crosstalk delay change analysis. In *IEEE/ACM International Conference on Computer Aided Design, 2004. ICCAD-2004.*, pages 147–154. IEEE, 2004.

[41] Peng Li and Emrah Acar. A waveform independent gate model for accurate timing analysis. In *2005 International Conference on Computer Design*, pages 363–365. IEEE, 2005.

[42] Hanif Fatemi, Shahin Nazarian, and Massoud Pedram. Statistical logic cell delay analysis using a current-based model. In *Proceedings of the 43rd annual Design Automation Conference*, pages 253–256, 2006.

[43] Chandramouli Kashyap, Chirayu Amin, Noel Menezes, and Eli Chiprout. A nonlinear cell macromodel for digital applications. In *2007 IEEE/ACM International Conference on Computer-Aided Design*, pages 678–685. IEEE, 2007.

[44] Noel Menezes, Chandramouli Kashyap, and Chirayu Amin. A" true" electrical cell model for timing, noise, and power grid verification. In *Proceedings of the 45th annual Design Automation Conference*, pages 462–467, 2008.

[45] Behnam Amelifard, Safar Hatami, Hanif Fatemi, and Massoud Pedram. A current source model for cmos logic cells considering multiple input switching and stack effect. In *Proceedings of the conference on Design, automation and test in Europe*, pages 568–573, 2008.

[46] Shahin Nazarian, Hanif Fatemi, and Massoud Pedram. Accurate timing and noise analysis of combinational and sequential logic cells using current source modeling. *IEEE transactions on very large scale integration (VLSI) systems*, 19(1):92–103, 2010.

[47] Naveen Kumar Katam and Massoud Pedram. Timing characterization for static timing analysis of single flux quantum circuits. *IEEE Transactions on Applied Superconductivity*, 29(6):1–8, 2019.

[48] Cadence Design Systems. Effective current source model (ecsm). Online. URL https://www.cadence.com/en_US/home/alliances/standards-and-languages/ecsm-library-format.html. Accessed: 2025-03-29.

[49] Florentin Dartu, Noel Menezes, and Lawrence T Pileggi. Performance computation for precharacterized cmos gates with rc loads. *IEEE Transactions on Computer-Aided Design of Integrated Circuits and Systems*, 15(5):544–553, 1996.

[50] Janet Meiling Wang, Jun Li, Satish Yanamanamanda, Lakshmi Kalpana Vakati, and Kishore Kumar Muchherla. Modeling the driver load in the presence of process variations. *IEEE Transactions on Computer-Aided Design of Integrated Circuits and Systems*, 25(10): 2264–2275, 2006.

[51] Andrew B Kahng and Sudhakar Muddu. Improved effective capacitance computations for use in logic and layout optimization. In *Proceedings Twelfth International Conference on VLSI Design.(Cat. No. PR00013)*, pages 578–582. IEEE, 1999.

[52] Muzhou Shao, Martin DF Wong, Huijing Cao, Youxin Gao, Li-Pen Yuan, Li-Da Huang, and Seokjin Lee. Explicit gate delay model for timing evaluation. In *Proceedings of the 2003 international symposium on Physical design*, pages 32–38, 2003.

[53] Dimitrios Garyfallou, Stavros Simoglou, Nikolaos Sketopoulos, Charalampos Antoniadis, Christos P Sotiriou, Nestor Evmorfopoulos, and George Stamoulis. Gate delay estimation with library compatible current source models and effective capacitance. *IEEE Transactions on Very Large Scale Integration (VLSI) Systems*, 29(5):962–972, 2021.

[54] Chirayu S Amin, Florentin Dartu, and Yehea I Ismail. Weibull-based analytical waveform model. *IEEE Transactions on Computer-Aided Design of Integrated Circuits and Systems*, 24 (8):1156–1168, 2005.

[55] Tao Lin, Emrah Acar, and Lawrence Pileggi. h-gamma: an rc delay metric based on a gamma distribution approximation of the homogeneous response. In *Proceedings of the 1998 IEEE/ACM international conference on Computer-aided design*, pages 19–25, 1998.

[56] Nahid Mirzaie and Ron Rohrer. A macromodeling approach for analog behavior of digital integrated circuits. *IEEE Transactions on Computer-Aided Design of Integrated Circuits and Systems*, 39(12):5025–5031, 2020.

[57] Jaideep Pathak, Brian Hunt, Michelle Girvan, Zhixin Lu, and Edward Ott. Model-free prediction of large spatiotemporally chaotic systems from data: A reservoir computing approach. *Physical review letters*, 120(2):024102, 2018.

[58] Bethany Lusch, J Nathan Kutz, and Steven L Brunton. Deep learning for universal linear embeddings of nonlinear dynamics. *Nature communications*, 9(1):4950, 2018.

[59] Naoya Takeishi, Yoshinobu Kawahara, and Takehisa Yairi. Learning koopman invariant subspaces for dynamic mode decomposition. *Advances in neural information processing systems*, 30, 2017.

[60] Alvaro Sanchez-Gonzalez, Jonathan Godwin, Tobias Pfaff, Rex Ying, Jure Leskovec, and Peter Battaglia. Learning to simulate complex physics with graph networks. In *International conference on machine learning*, pages 8459–8468. PMLR, 2020.

[61] Haoyi Zhou, Shanghang Zhang, Jieqi Peng, Shuai Zhang, Jianxin Li, Hui Xiong, and Wancai Zhang. Informer: Beyond efficient transformer for long sequence time-series forecasting. In *Proceedings of the AAAI conference on artificial intelligence*, volume 35, pages 11106–11115, 2021.

[62] Shai Shalev-Shwartz and Shai Ben-David. *Understanding Machine Learning: From Theory to Algorithms*. Cambridge University Press, 1st edition, 2014.

[63] James Stewart. *Calculus: Early Transcendentals*. Cengage Learning, 8th edition, 2015.

[64] Peter L. Bartlett and Shahar Mendelson. Rademacher and gaussian complexities: Risk bounds and structural results. *Journal of Machine Learning Research*, 3:463–482, 2002.

[65] Mehryar Mohri, Afshin Rostamizadeh, and Ameet Talwalkar. *Foundations of Machine Learning*. MIT Press, 2nd edition, 2018.

Appendix Contents

- **A.** Related Works
  - A.1 Background
  - A.2 Traditional Methods for Signal Line RC Response Modeling
  - A.3 Current Applications of Neural Networks in Modeling Nonlinear Systems
- **B.** Dataset Preparation Details
  - B.1 Reference Simulator for Ground-Truth Generation
  - B.2 Dataset Computing Environment
  - B.3 Dataset Preparation
    - B.3.1 Netlist Generation
    - B.3.1.1 Circuit Structure
    - B.3.2 Automated HSPICE Simulation and Parser
    - B.3.3 Function Extraction
      - 1. Netlist Parsing
      - 2. State-Space Model Construction
      - 3. Transfer-Function Computation
      - 4. Result Serialization
  - B.4 Data Alignment
- **C.** Log-Centered Time Warping & Resampling
  - C.1 Motivation
  - C.2 Center Detection
  - C.3 Log-Centred Warping
  - C.3.1 Slope Compression
  - C.4 Uniform Resampling in the Warped Domain
  - C.5 Effect of Uniform Resampling on Regression Accuracy
  - C.6 Theoretical Impact on Learning
  - C.7 Proof of Lipschitz Constant Reduction
    - 1. Composition Lemma
    - 2. Derivative of the Inverse Warp
    - 3. Parameter Choice for Contraction
    - 4. Impact on Generalisation
  - C.8 Implementation Details
- **D.** Full Test Case
  - D.1 Training Data Preparation
  - D.2 First-Order Model Training and Error-Model Generation
  - D.3 Performance Evaluation
- **E.** 200-Order Extrapolation Results
  - E.1 Experimental Setup
  - E.2 Aggregate Metrics and Case Studies
  - E.3 Discussion and Limitations

A Related Works

A.1 Background

Modeling and simulation of high-order nonlinear systems remain central challenges in modern VLSI backend design, particularly in analog/mixed-signal verification and large-scale circuit time-domain modeling. Mainstream industrial tools such as HSPICE predominantly rely on Newton-Raphson iterative solvers coupled with numerical integration schemes like Gear or Trapezoidal methods. While these solvers offer high physical accuracy, their simulation time and resource consumption scale poorly with system complexity-especially in the presence of strong nonlinearities or high-order dynamics-posing significant computational bottlenecks for practical deployment.

In recent years, neural networks have demonstrated remarkable success across a wide range of scientific computing applications, including areas within electronic design automation (EDA) such as device modeling [37], analog circuit fault detection [38], and high-frequency electromagnetic simulation [39]. However, for the specific task of modeling signal line RC responses in high-order nonlinear systems, effective deep learning-based approaches remain largely unexplored. To the best of our knowledge, no existing work has leveraged deep neural networks-particularly Transformer-based architectures-for direct time-domain modeling of such systems.

Given this gap, we provide a comprehensive review of related work from two perspectives: (1) traditional modeling approaches developed in the EDA community for approximating RC signal line responses, including current source models, voltage response models, and direct waveform fitting methods; and (2) recent advances in neural network-based methods for modeling general nonlinear dynamical systems, which-while related in scope-target different modeling granularities and lack direct applicability to high-order S-domain waveform prediction.

A.2 Traditional Methods for Signal Line RC Response Modeling

Existing methods for modeling signal line RC response can be broadly classified into three categories:

The first category is the Current Source Model (CSM). Criox and Wong proposed a gate cell current source model called Blade [20], which consists of a voltage-controlled current source, internal capacitance, and a one-step time-shift operation. Kellor further enhanced model accuracy by introducing the KTV model [40], which considers Miller capacitance. Subsequently, Li and Acar [41] and Fatemi et al. [42] introduced input and output parasitic capacitances, modeling the output current source as a function of input/output voltages, gradually incorporating nonlinear characteristics into CSM models. However, since CSM-based methods can only match fixed effective capacitances (up to two) throughout the process, the simulation accuracy of current/voltage waveforms is inherently limited [24][43][44][45][46][47] . In recent years, widely adopted industry methods such as Composite Current Source (CCS) [21] and Extended Current Source Model (ECSM) [48] have established driver and receiver models for each cell to handle scenarios with nonlinear input and crosstalk. Nevertheless, CSM-based approaches still face significant challenges in matching high-order RC load characteristics, limiting their accuracy in current response prediction.

The second category is the Voltage Response Model (VRM), such as the Non-Linear Delay Model (NLDM). Iterative methods [22] [25] [49] [50] , although capable of achieving high precision, often require substantial CPU time for convergence. Non-iterative methods [51] [52], on the other hand, rely on closed-form expressions that offer faster computation but can result in output waveform matching errors of up to 15% [26]. Furthermore, as technology nodes shrink and RC loads become more complex, two-parameter fitting methods struggle to accurately capture the response curve of RC networks, limiting their applicability in high-precision simulations [53].

The third category consists of Direct Waveform Prediction Methods, such as double exponential functions [23], Weibull functions [54], and gamma functions [55], which directly fit the current or voltage response. Recently, a macromodeling method [56] was proposed that uses SPICE to extract parameters for modeling, which improves accuracy to some extent. However, these direct fitting methods are unable to predict initial overshoot/undershoot effects, which become more pronounced when the input slope is large.

A.3 Current Applications of Neural Networks in Modeling Nonlinear Systems

In recent years, neural networks have been widely applied to modeling and prediction tasks of nonlinear dynamical systems. Neural ODE methods [12] introduce continuous-time differential equations to model system evolution, which are suitable for trajectory prediction problems. Physics-Informed Neural Networks (PINNs) [11] incorporate partial differential equation constraints during training to enhance physical consistency of the model. Additionally, Reservoir Computing [57] has demonstrated excellent performance in modeling short-term behavior of chaotic systems, while Koopman operator learning [58, 59] attempts to linearize nonlinear systems by mapping them into a linear space to simplify modeling. Graph Neural Networks (GNNs) [60] process complex local interactions by constructing graphs among components, and neural operator methods, such as the Fourier Neural Operator (FNO) [14] and DeepONet [13], focus on learning mappings of high-dimensional functions. In the domain of time series forecasting, Transformer-based models and their variants (e.g., Informer [61]) have demonstrated strong capability in modeling long-term dependencies. Although these methods have achieved substantial progress in various scientific computing scenarios, existing works mainly focus on low-dimensional systems, continuous trajectory modeling, or frequency-domain PDE solving, with limited exploration in modeling high-order time-domain responses of complex circuit RC networks.

The proposed S-Crescendo framework in this work possesses three key characteristics designed to effectively model time-domain behaviors in high-order nonlinear systems. First, it explicitly separates system modes via partial fraction decomposition of the S-domain transfer function. Second, it employs a distributed Transformer architecture combined with pole-residue embedding strategies, reducing the response prediction complexity from cubic $\mathcal{O}(n^3)$ to linear $\mathcal{O}(n)$. Third, it introduces an attention-based correction operator that adaptively captures nonlinear coupled responses while modeling dominant modes. This framework combines physical interpretability with computational efficiency and demonstrates high-fidelity waveform fitting consistent with HSPICE simulations on validation datasets, thus filling the gap of deep learning-based modeling for high-order circuit systems.

B Dataset Preparation Details

B.1 Reference Simulator for Ground-Truth Generation

All training and evaluation datasets in this work are generated using Synopsys PrimeSim HSPICEő U2023.03SP22. HSPICE is widely acknowledged as the de facto industry reference for analog and mixed-signal circuit simulation, owing to its consistently strong agreement with post-silicon measurementstypically achieving within 1%-5% error across a broad range of process nodes (from 0.18 µm to 3 nm). It provides foundry-certified transistor and passive device models, enabling high physical fidelity and process portability. Moreover, its Precision Parallel simulation engine supports near-linear scalability on multi-core systems such as the AMD EPYC 7763 (64-core), facilitating efficient, high-accuracy waveform generation even for large-scale nonlinear networks. These capabilities establish HSPICE as a trusted ground-truth generator for validating data-driven modeling frameworks.

B.2 Dataset Computing Environment

The experiments were conducted on a computing platform running CentOS Linux 7, an operating system known for its long-term stability and high compatibility with the source code of Red Hat Enterprise Linux (RHEL). This ensures the reliability and consistency of the system environment, facilitating reproducibility of the experimental results.

The hardware platform is equipped with an AMD EPYC 7763 processor, featuring 64 physical cores with a base clock frequency of 2.45 GHz and dynamic boost up to 3.5 GHz. It includes a 256 MB L3 cache and an 8-channel DDR4-3200 MT/s memory architecture, providing substantial parallel computing capability and high memory bandwidth. This configuration offers ample computational resources and efficient data handling, guaranteeing smooth execution of large-scale simulation workloads while minimizing potential performance bottlenecks.

B.3 Dataset Preparation

The dataset was constructed through a multi-stage pipeline. First, a Python script automatically generated SPICE netlists (".sp" files) representing RC networks of varying orders. These netlists were then processed along two parallel paths. In the first path, a Python module parsed each netlist to compute the corresponding analytical transfer function. In the second path, all netlists were batch-simulated using PrimeSim HSPICE U-2023.03-SP2-2 to obtain time-domain simulation results. Upon completion of the simulations, another Python script extracted the relevant outputs from the HSPICE raw data files. Finally, the analytical transfer functions and the corresponding simulated results were aligned and merged into a unified dataset, which served as the basis for subsequent model training and evaluation (see Figure 5).

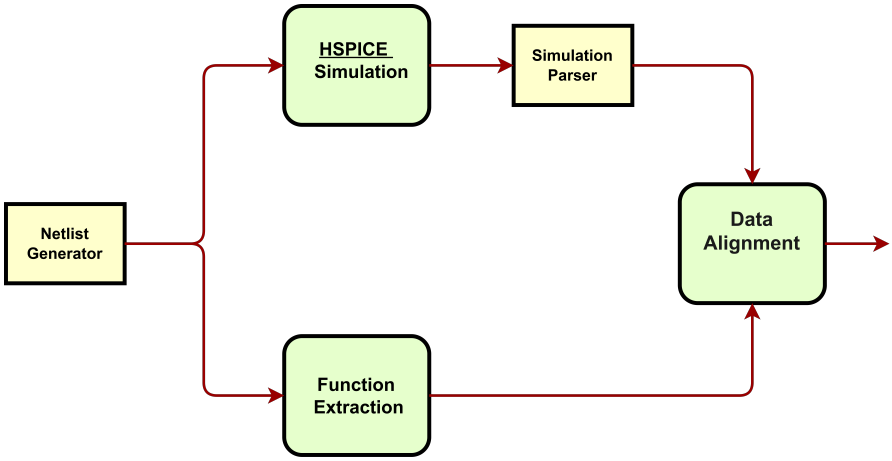

Figure 5: Overview of the dataset preparation pipeline.

B.3.1 Netlist Generation

A Python script automatically generates SPICE netlists for cascaded RC networks of arbitrary order. For first-order RC circuits, we adopt an exhaustive grid-based method by varying R_1 and C_1 across predefined intervals to construct a comprehensive dataset that covers a wide range of transfer functions. The script iterates over discrete values and generates files named `testsuite_<n>.sp`, each invoking a transient simulation (`.TRAN 10ps 20ns`) and including standard PDK models to ensure consistency.

For higher-order RC networks ($N > 1$), due to the exponential growth in parameter space, exhaustive enumeration becomes computationally infeasible. Instead, we construct a continuous state space defined by all possible tuples $\{R_n, C_n\}_{n=1}^{N}$, and sample from this space using randomized or quasi-random strategies. Each sample corresponds to a specific configuration of RC parameters, which is then used to generate a netlist representing an Nth-order cascaded RC system. This hybrid strategy ensures both completeness in low-order cases and scalability in high-order scenarios, providing a diverse and representative dataset for model training and evaluation.

The dataset generation scripts and usage examples are available at our code in supplemental_material.zip.

Circuit structure We construct a canonical nonlinearlinear cascade by driving a linear RC network with a nonlinear inverter. The nonlinear frontend is implemented as a standard-cell inverter in SPICE:

```
X1 I1 OUT vdd 0 CLKINV3_12TR50
```

Here, `OUT` is the inverters output node, which serves as the input to the linear RC load. In the simplest first-order configuration, the RC network consists of a single resistorcapacitor pair:

```
R1 OUT          NODE1    r1
C1 NODE1        0        c1
```

To generalize this to an N-stage cascade, we chain N identical first-order sections. Each section n is defined in the netlist as:

```
R1 OUT         NODE1     r1
C1 NODE1       0         c1

⋮

R<n> NODE<n-1> NODE<n>  r<n>
C<n> NODE<n>   0        c<n>
```

where the nodes are labeled sequentially as `NODE0=OUT`, `NODE1`, , `NODE`n, and `NODE`n is grounded.

Although a single stage has the well-known transfer function

$$H_n(s) = \frac{1}{1 + sR_nC_n},$$

the overall transfer function of the cascaded network cannot be written as the simple product $\prod_{n=1}^{N} H_n(s)$. Inter-stage couplingwhere each stages output drives the nextrequires solving the full circuit equations or deriving a state-space model to obtain $H(s)$ correctly.

Once the high-order transfer function $H(s)$ is obtained, we apply *partial fraction expansion* (PFE) to decompose it into modal contributions:

$$H(s) = \sum_{k=1}^{N} \frac{r_k}{s - p_k},$$

where p_k and r_k denote the poles and residues, respectively. This modal form explicitly exposes the dynamic modes of the network and forms the theoretical foundation for our S-domainaware Transformer model in time-domain prediction of high-order nonlinear circuits.

B.3.2 Automated HSPICE Simulation and Simulation Parser

The HSPICE simulation workflow was fully automated via a Python script that sequentially runs all SPICE netlists. Each simulation outputs transient voltage responses at the designated output node, saved in `.lis` files containing detailed time-domain voltage and current waveforms.

To facilitate efficient data extraction and downstream processing, a dedicated Python parser was implemented to systematically extract voltage response sequences from these `.lis` files. A representative snippet of the extracted data is shown below:

```
time         voltage
0.000000e+00 1.8579u
1.000000e-11 9.7816m
2.000000e-11 1.78649e-02
3.000000e-11 2.54157e-02
4.000000e-11 3.26519e-02
5.000000e-11 3.79554e-02
6.000000e-11 4.32588e-02
```

These extracted voltage traces serve as ground truth data for validating the analytical transfer functions and for subsequent model training and evaluation.

B.3.3 Function Extraction

To characterize the linear dynamics of cascaded RC networks, we implemented a fully automated Python pipeline comprising four stages: netlist parsing, state-space construction, transfer-function computation, and result serialization.

1. Netlist Parsing Using regular expressions, the parser reads each SPICE file to extract resistor R_i and capacitor C_i values. For a third-order network, the script locates lines beginning with `R1`, `R2`, …, `C3` and applies unit-aware conversion (e.g., `f`10^{-15}, `u`10^{-6}). Missing or malformed entries trigger an exception to ensure data integrity.

2. State-Space Model Construction Given the extracted $\{R_i, C_i\}$, an admittance matrix $G \in \mathbb{R}^{3\times 3}$ and capacitance matrix C_{diag} are assembled for the 3-stage RC ladder. The continuous-time state-space matrices are then computed as

$$\mathbf{A} = -C_{\text{diag}}^{-1} G, \quad \mathbf{B} = C_{\text{diag}}^{-1} [\, 1/R_1,\, 0,\, 0 \,]^{\mathsf{T}}, \quad \mathbf{C} = [\, 0,\, 0,\, 1 \,].$$

3. Transfer-Function Computation The transfer function $H(s)$ is obtained from $(\mathbf{A}, \mathbf{B}, \mathbf{C})$ via SciPys `ss2tf` routine, yielding numerator and denominator polynomials. We apply partial-fraction expansion (`residue`) to extract poles p_i and residues r_i. After filtering negligible imaginary parts, poles are sorted by magnitude, and normalized coefficients are computed as

$$A'_i = -\frac{r_i}{p_i}, \quad A'_i \leftarrow \frac{A'_i}{\sum_j A'_j}.$$

4. Result Serialization For each netlist, the tuple $(A'_1, p_1, A'_2, p_2, A'_3, p_3)$ is written as a single row in a CSV file. This standardized format enables downstream training pipelines to ingest model parameters directly.

B.4 Data Alignment

To prepare the dataset for sequence modeling tasks, we concatenate the static circuit features with the time-dependent voltage response while preserving the temporal dimension explicitly.

Let $\mathbf{x} \in \mathbb{R}^{2n}$ denote the RC feature vector extracted from an n-th order RC network (e.g., normalized residues and poles). For a third-order network, we have:

$$\mathbf{x} = (A'_1, p_1, A'_2, p_2, A'_3, p_3) \in \mathbb{R}^6.$$

Let the voltage response sequence over T time steps be represented as a set of timestamped scalar pairs:

$$\{(t_1, y_1), (t_2, y_2), \ldots, (t_T, y_T)\}, \quad \text{where } y_t \in \mathbb{R},\ t_t \in \mathbb{R}.$$

To incorporate both dynamic and static information, we replicate the static vector $\mathbf{x}$ at each time step and form the augmented matrix:

$$\mathbf{z}(t) = \begin{bmatrix} t_1 & y_1 & \mathbf{x} \\ t_2 & y_2 & \mathbf{x} \\ \vdots & \vdots & \vdots \\ t_T & y_T & \mathbf{x} \end{bmatrix} \in \mathbb{R}^{T\times(2+2n)}.$$

This results in a fully timestamped sequence $\mathbf{z}(t)$, where each row consists of:

- the current simulation time t_t,
- the corresponding voltage response y_t,
- and the circuit's physical parameters $\mathbf{x}$.

Such a format allows temporal models to condition predictions not only on voltage dynamics but also on circuit-specific properties.

All datasets were automatically constructed using a Python script that fuses the time vector, voltage response, and RC features.

C Log-Centered Time Warping & Uniform Resampling

C.1 Motivation

A step response $v(t)$ typically exhibits an extremely steep leading edge followed by a long, almost flat settling tail. When the raw waveform is sampled on a *linear* time axis, the number of informative points located on the rising edge is orders of magnitude smaller than the points on the tail. Consequently, regression models trained with a uniform loss (e.g. MSE) tend to *under-fit* the neighbourhood of the edge and over-fit the low-slope region, yielding poor predictions for signals whose rise times differ markedly inside the same simulation window.

C.2 Center detection

Let t_c be the time at which the normalised voltage first crosses $v = 0.5$:

$$v(t_c) = \tfrac{1}{2}V_{\mathrm{DD}}, \qquad t_c = \arg\min_t \left|v(t) - \tfrac{1}{2}V_{\mathrm{DD}}\right|.$$

The algorithm finds t_c with a twostage linear B-spline interpolation around the crossing (see `find_t()` in the accompanying code base).

C.3 Log-centred warping

For every sample t we define a *log-centred* time coordinate

$$\tau \;=\; \mathrm{sgn}\big(t - t_c\big)\,\Big[\ln\big(|t - t_c|/T_0 + \varepsilon\big) - \ln\varepsilon\Big], \tag{13}$$

with scale factor $T_0 = 10^{-10}$ s (empirically chosen) and numerical guard $\varepsilon = 0.1$. Equation (13) is *odd* around t_c and strictly monotone; consequently the mapping $t \mapsto \tau$ is invertible and preserves temporal order.

Slope compression. The first derivative

$$\frac{d\tau}{dt} \;=\; \frac{1}{|t - t_c| + \varepsilon T_0}$$

is large when $|t - t_c|$ is small and diminishes as $|t - t_c| \to \infty$. Hence points on the steep edge ($|t - t_c| \ll T_0$) are *stretched* in τ-space while the quasi-flat tail is *compressed*. In effect, the dynamic range of local slopes

$$\left|\tfrac{dv}{dt}\right| \;\longrightarrow\; \left|\tfrac{dv}{d\tau}\right| = \left|\tfrac{dv}{dt}\right| \frac{dt}{d\tau} \;=\; \left|\tfrac{dv}{dt}\right| \big(|t - t_c| + \varepsilon T_0\big)$$

is equalised, yielding a better-conditioned learning target.

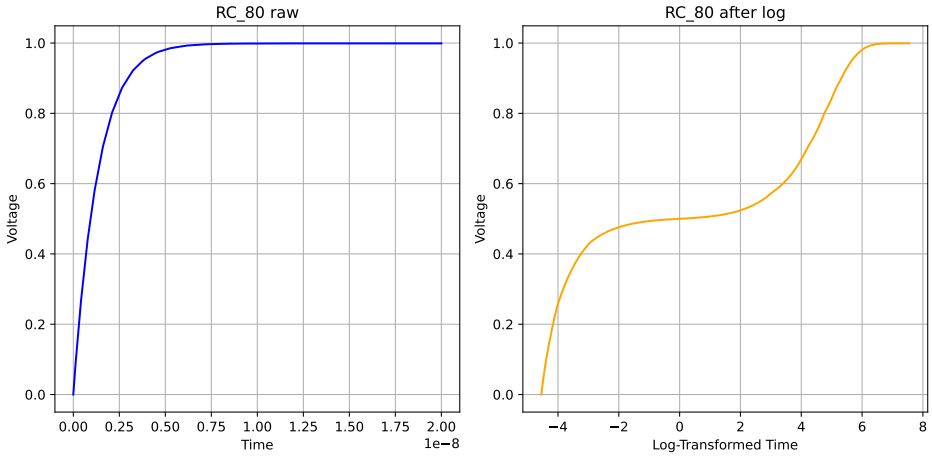

Figure 6: Raw waveform vs. log-centred waveform.

C.4 Uniform resampling in the warped domain

After warping, we resample the trace at N *equally spaced* τ-locations

$$\tau_k = \tau_{\min} + k\Delta\tau, \quad k = 0, \ldots, N-1, \qquad \Delta\tau = \frac{\tau_{\max} - \tau_{\min}}{N - 1}.$$

Linear interpolation in τ-space is equivalent to *non-uniform* interpolation in the original time domain, so the final dataset allocates identical representational capacity to equal increments of τ, i.e. to equal *log-scaled* time gaps with respect to the edge.

Figure 7 shows: (a) The original voltage response $v(t)$ for the first RC channel plotted against real time t. (b) The same trace after applying the center-log warp $t \mapsto \tau$ and uniformly resampling in τ-space. Black circles indicate the new sample locations, illustrating the denser coverage near the rising edge and sparser coverage on the tail.

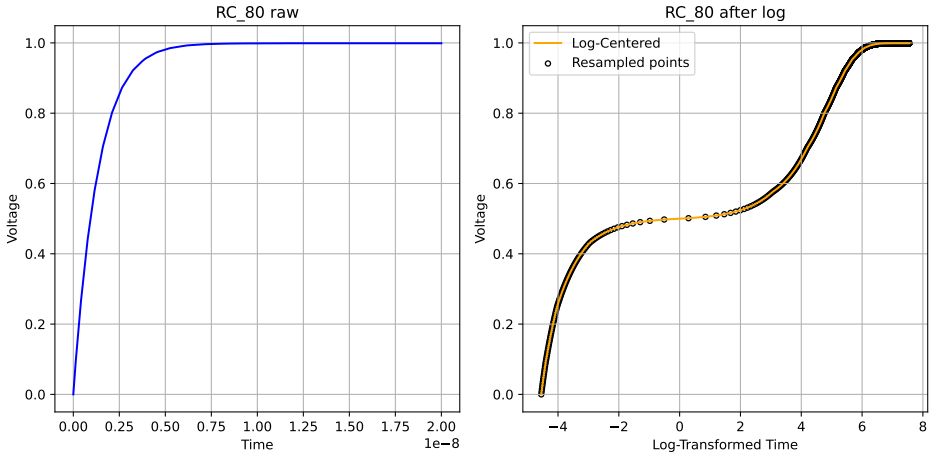

Figure 7: Scatter plot in τ-space: before vs. after resampling.

Comparison of the original step response and the uniform resampling in log-time domain. The blue markers show the raw voltage trace $v(t)$ for the RC network sample (from Figure 8), plotted against the log-centered time coordinate τ. The orange markers overlay the uniformly spaced samples in τ-space, demonstrating that the resampling allocates more points near the steep rising edge while compressing the long tail.

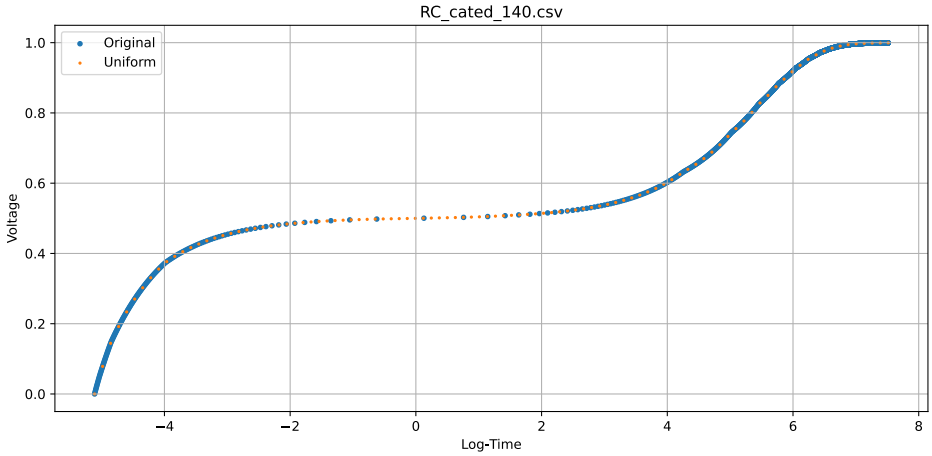

Figure 8: Scatter plot in τ-space: resampling vs. after uniformed resampling.

C.5 Effect of Uniform Resampling on Regression Accuracy

We conducted an experiment to quantify the impact of our logcentered warping *plus* uniform resampling on stepresponse modelling accuracy. Under identical training conditions: 60 epochs, batch size = 1000, using 80 training files (80 Œ 1000 samples) drawn from the full set of 100 RC cases. The model was evaluated on the held-out test set comprising cases RC_81 through RC_100. We report the coefficient of determination R^2 for predictions made with ("Resampled") and without ("Raw") the uniform resampling in warped time.

Table 3: R^2 comparison: raw vs. logcentered τ-uniform resampling.

Case	R^2 Raw	R^2 Resampled
RC_81	0.9571	0.9998
RC_82	0.9591	0.9998
RC_83	0.9609	0.9998
RC_84	0.9629	0.9998
RC_85	0.9647	0.9998
RC_86	0.9662	0.9998
RC_87	0.9675	0.9998
RC_88	0.9690	0.9998
RC_89	0.9702	0.9998
RC_90	0.9714	0.9998
RC_91	0.9725	0.9998
RC_92	0.9736	0.9998
RC_93	0.9745	0.9998
RC_94	0.9753	0.9998
RC_95	0.9761	0.9998
RC_96	0.9768	0.9998
RC_97	0.9774	0.9998
RC_98	0.9780	0.9998
RC_99	0.9785	0.9999
RC_100	0.9816	0.9999
Mean	0.9715	0.9998

Qualitatively, Table 3 shows that uniform resampling in τ-space consistently boosts R^2 from the high-0.95 range up to nearly perfect 0.999. On average, the preprocessing yields an absolute improvement of over 0.028 in R^2, demonstrating that our logcentered warp and uniform sampling dramatically enhances the models ability to fit diverse stepresponse curves under identical training regimes.

As shown in Figure 9, we compare the predictive accuracy of our network on the same RC trace under two preprocessing regimes. In subfigure 9a, the model is trained and evaluated directly on the raw time-domain samples, achieving an R^2 of 0.9571. While the overall step response shape is captured, the prediction exhibits noticeable lag on the steep rising edge and slight deviation in the mid-tail region. In contrast, subfigure 9b illustrates the result after applying the center-log warping followed by uniform resampling in the warped τ-domain. Here, the fit improves dramatically to an R^2 of 0.9998, with the predicted curve (orange) virtually indistinguishable from the ground truth (blue) across both the fast edge and the extended settling tail. This comparison clearly demonstrates that our log-centering and uniform resampling pipeline substantially enhances the models ability to learn and generalize step-response dynamics under identical training conditions.

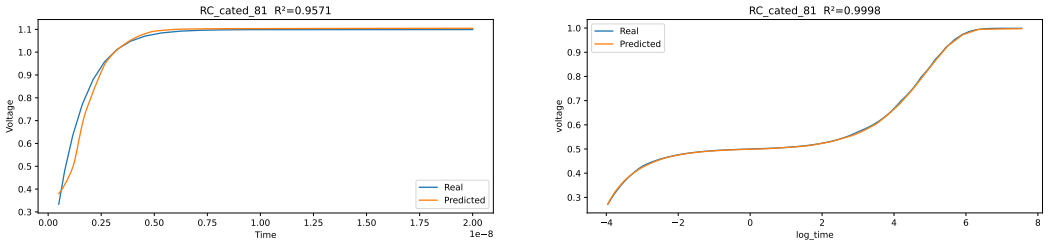

(a) Original time-domain fit (R^2=0.9571). (b) Log-time fit after preprocessing (R^2=0.9998).

Figure 9: Model predictions vs. ground truth for two RC traces: (a) raw time-domain input, (b) preprocessed (center-log warp + uniform resampling) input.

C.6 Theoretical impact on learning

- **Variance reduction.** Let σ^2_{raw} denote the variance of the target derivative $\frac{dv}{dt}$ on the raw grid and σ^2_{warp} the variance of $\frac{dv}{d\tau}$ on the warped grid. From the slope-compression term above it follows that $\sigma^2_{\text{warp}} \leq \sigma^2_{\text{raw}}$, reducing heteroscedasticity seen by the learner.
- **Effective sample size (ESS).** The warping acts as an *importance-sampling* scheme with weight $w(t) = |t - t_c| + \varepsilon T_0$. ESS increases because highly informative edge samples receive larger weights after transformation.
- **Improved Lipschitz constant.** Denote the network f_θ with Lipschitz constant L. The composite function $f_\theta \circ g^{-1}$ (where g^{-1} is the inverse warp) retains the same L but is now evaluated on a domain where the target variation is smaller, tightening generalisation bounds.

C.7 Proof of Lipschitz Constant Reduction

We now show that, under mild parameter choices, the pre-/post-warp composite

$$F(\tau) \;=\; f_\theta\big(g^{-1}(\tau)\big)$$

has an overall Lipschitz constant $L' < L$.

1. Composition lemma. If $f : X \to Y$ is L_f-Lipschitz and $h : Z \to X$ is L_h-Lipschitz, then

$$\|f \circ h(z_1) - f \circ h(z_2)\| \;\leq\; L_f \,\|h(z_1) - h(z_2)\| \;\leq\; L_f \, L_h \,\|z_1 - z_2\|,$$

so $f \circ h$ is $L_f L_h$-Lipschitz [62].

2. Derivative of the inverse warp. Recall the forward warp

$$\tau = g(t) = \operatorname{sgn}(t - t_c)\Big[\ln\big(\tfrac{|t-t_c|}{T_0} + \varepsilon\big) - \ln \varepsilon\Big].$$

Differentiating,

$$\frac{d\tau}{dt} = \frac{1}{|t - t_c| + \varepsilon\, T_0} \implies \frac{dt}{d\tau} = |t - t_c| + \varepsilon\, T_0.$$

Since a one-dimensional C^1 function h with $\sup |h'(x)| \leq M$ is M-Lipschitz by the Mean Value Theorem [63], it follows that

$$L_{g^{-1}} = \sup_{\tau \in [\tau_{\min}, \tau_{\max}]} \left|\tfrac{d\, g^{-1}}{d\tau}\right| = \sup_{t \in [t_{\min}, t_{\max}]} \big(|t - t_c| + \varepsilon\, T_0\big).$$

3. Parameter choice for contraction. Let $\Delta t = \max\{|t_{\max} - t_c|, |t_{\min} - t_c|\}$. If we choose parameters so that

$$\Delta t + \varepsilon\, T_0 < 1,$$

then

$$L_{g^{-1}} < 1 \quad\Longrightarrow\quad L' = L_{f_\theta}\, L_{g^{-1}} < L_{f_\theta}.$$

Hence $F(\tau)$ is strictly more contractive than f_θ on the original t-domain.

4. Impact on generalisation. Standard Rademachercomplexity generalisation bounds scale linearly with the Lipschitz constant of the hypothesis class and inversely with $\sqrt{N}$ [64, 65]. By reducing the effective Lipschitz constant from L to $L' < L$, we tighten the bound

$$\mathcal{E}_{\text{gen}} = O\Big(\tfrac{L'}{\sqrt{N}}\Big) \;\subset\; O\Big(\tfrac{L}{\sqrt{N}}\Big),$$

thereby improving expected test performance.

C.8 Implementation details

1. **Voltage normalisation.** All voltages are scaled by V_{DD} so that $v \in [0, 1]$.
2. **Time origin.** Warping is performed *after* shifting the origin to t_c. This removes sample-to-sample phase variation.
3. **Parameter choices.** T_0 controls the width of the expanded region; in our experiments ($10^{-10}s$) adequately covers modern technology nodes down to 3 ps edges.

D Full Test Case

D.1 Training Data Preparation

Netlist Generation

- Prepare a pool of base RC parameter pairs
- Run:

```
python prepare/n.py \
  --order n \
  --count m \
  --output_dir sp_files_n
```

HSPICE Simulation

- Simulations are executed via `sim.sh` under Linux.
- Run:

```
hspice testsuite_<n>.sp -o lis/result_<n>
```

  Simulation outputs are stored in the `lis/` directory.

Simulation Parser

- Place your HSPICE `.lis` files into the `./result/` directory.
- Run the parsing script to extract time-voltage waveforms and convert units:

```
python parse_spice.py \
--input_dir ./result \
--output_dir ./result/csv/
```

- Parsed CSV files will be saved in `./result/csv/` for further analysis.

Function Extraction

- Place your SPICE netlist files (`.sp`) into the directory `sp_files_n/`.
- Run the extraction script to parse resistor and capacitor values, compute state-space parameters, poles, and residues:

```
python extract_functions.py \
--input_dir sp_files_n \
--output_dir result_n
```

- The extracted normalized residues A'_i and poles p_i for each netlist are saved as CSV files in `result_n/`.

Data Alignment

- Place your RC parameter CSVs in `RC/` and parsed SPICE result CSVs in `lis/result/`.
- Run the script to merge each pair into `result/` as follows:

```
python data_alignment.py
```

- This script reads the first row from each RC CSV, duplicates it to match the length of the corresponding SPICE CSV, concatenates them column-wise, and saves the combined CSV.
- Processed files are named `RC_cated_i.csv` for $i = 1, \ldots, n$.

D.2 First-Order Model Training and Error-Model Generation

The following workflow describes how to train the firstorder predictor and automatically generate the residual (error) datasets for higher-order correction models. All commands assume you are in the repository root (see code in supplemental_material.zip).

1. **Log-centred warp & resampling for Model 1 data**
   - Place your pre-factorised first-order training CSVs into `testxiao/basic/model1/`.
   - Run:

     ```
     python testxiao/testxiao.py \
       --input_dir testxiao/basic/model1 \
       --output_dir testxiao/results \
       --warp center-log
     ```

     Intermediate warped traces appear in `testxiao/results/`.
   - Next, uniformly resample in τ-space:

     ```
     python testxiao/uniform.py \
       --input_dir testxiao/results \
       --output_dir data/model1
     ```

     The resampled CSVs for Model 1 are now in `data/model1/`.
2. **Train the first-order model**
   - Launch training:

     ```
     python train_model1.py \
       --data_dir data/model1 \
       --save_path models/static_cond_model.pth
     ```

     Upon completion, the static first-order model is saved as `models/static_cond_model.pth`.
3. **Generate error datasets**
   - Execute the pipeline script to compute residuals:

     ```
     python pipeline_train_error_models.py \
       --model_path models/static_cond_model.pth \
       --input_dir data/model1 \
       --tmp_dir _tmp_ds
     ```

     This creates erroroforder-2 and erroroforder-3 traces in `_tmp_ds/`.
   - Copy the intermediate error files into the next data folder:

     ```
     cp _tmp_ds/error_*.csv data/error/
     ```
4. **Train the error models**
   - Finally, train the error prediction networks:

     ```
     python combine_and_train_error_model.py \
       --data_dir data/error \
       --save_prefix models/model_error
     ```

     This produces `models/model_error_2.pth` and `models/model_error_3.pth`, which predict the 2nd- and 3rd-order residuals respectively.

All script invocations include detailed usage notes in their headers. For full examples and parameter options, consult the source files in the `testxiao/` and root directories of our code in supplemental_material.zip

D.3 Performance Evaluation

Once the static and error models have been trained (`models/static_cond_model.pth` and `models/model_error_n.pth`), we run the recursive inference script to generate test predictions and metrics. You may adjust inference parameters (e.g. batch size, lookback window) via command-line flags.

```
python test_recursive_inference.py \
  --data_dir    data/order1/test  \
  --static_model models/static_cond_model.pth \
  --err_model    models/model_error_n.pth   \
  --out_dir     results
```

The script outputs:

- Predicted vs. true response CSVs in `results/`
- Summary (R^2) printed to console and saved under `results/metrics/`
- Plots of stepresponse comparisons in `results/plots/`

E 200-Order Extrapolation for Dynamic Signoff

To address the dynamic signoff mode, we conducted high-order experiments up to 200 poles. We trained residual-correction modules on systems with no more than 15 poles and evaluated on a 200-pole network. The model achieved a coefficient of determination of $R^2 = 0.9838$, indicating that our approach scales to orders required for full dynamic signoff with a still manageable training cost (approximately 5–6 hours on a single RTX 4090).

E.1 Experimental Setup

We first generated training data for systems of order ≤ 15 using standard *HSPICE* simulations. Residual-correction modules contained approximately 100–160K parameters and were trained with mixed precision on a single NVIDIA RTX 4090 GPU. Hyperparameters followed the settings used in lower-order experiments (optimizer, learning rate schedule, batch size), with early stopping based on validation R^2. The 200-pole evaluation network was held out from training and tuned to match the transient signoff configuration (10 ns horizon, 1,000 samples).

E.2 Case Studies

We report aggregate metrics and qualitative comparisons against *HSPICE* on the 200-pole network. The model attains $R^2 = 0.9838$ with low mean absolute error and well-behaved residuals across the transient window. Visual overlays show close alignment at both fast and slow time scales, with the largest errors concentrated near rapid slope changes.

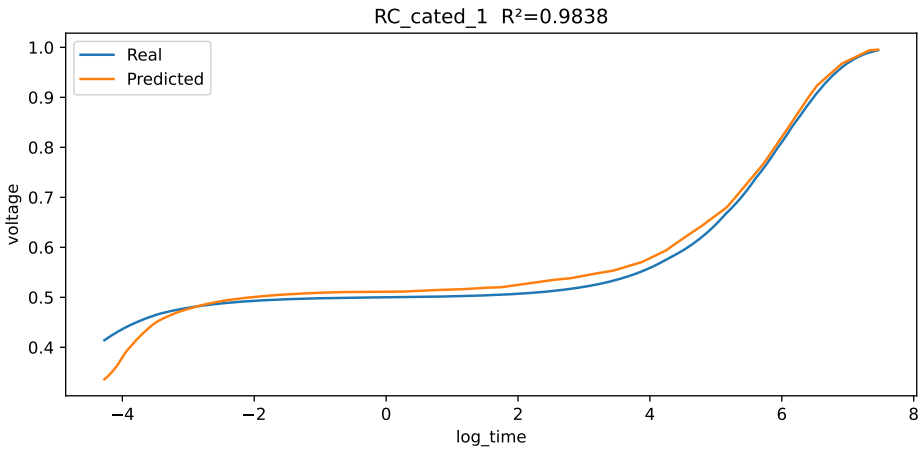

Figure 10: 200 order case study

E.3 Discussion

These results demonstrate that the residual-correction design generalizes beyond the training order range, providing stable extrapolation to 200 poles. While inference remains fast and memory-efficient, training cost scales primarily with data volume and sequence length; the reported 5–6 hours is a one-time training cost and remains practical for signoff contexts. Remaining gaps are localized to high-curvature regions, suggesting that targeted augmentation (e.g., emphasizing rapid transients) and modest architecture scaling could further close the accuracy margin without compromising the observed efficiency benefits.

NeurIPS Paper Checklist

1. **Claims**

   Question: Do the main claims made in the abstract and introduction accurately reflect the paper's contributions and scope?

   Answer: [Yes]

   Justification: The abstract and introduction clearly state the key contributions of the paper.

   Guidelines:

   - The answer NA means that the abstract and introduction do not include the claims made in the paper.
   - The abstract and/or introduction should clearly state the claims made, including the contributions made in the paper and important assumptions and limitations. A No or NA answer to this question will not be perceived well by the reviewers.
   - The claims made should match theoretical and experimental results, and reflect how much the results can be expected to generalize to other settings.
   - It is fine to include aspirational goals as motivation as long as it is clear that these goals are not attained by the paper.

2. **Limitations**

   Question: Does the paper discuss the limitations of the work performed by the authors?

   Answer: [Yes]

   Justification: The paper discusses limitations including error accumulation and explosive data requirements of this work in the beginning of Section 6, and provides further explanations and solutions in the rest of Section 6.

   Guidelines:

   - The answer NA means that the paper has no limitation while the answer No means that the paper has limitations, but those are not discussed in the paper.
   - The authors are encouraged to create a separate "Limitations" section in their paper.
   - The paper should point out any strong assumptions and how robust the results are to violations of these assumptions (e.g., independence assumptions, noiseless settings, model well-specification, asymptotic approximations only holding locally). The authors should reflect on how these assumptions might be violated in practice and what the implications would be.
   - The authors should reflect on the scope of the claims made, e.g., if the approach was only tested on a few datasets or with a few runs. In general, empirical results often depend on implicit assumptions, which should be articulated.
   - The authors should reflect on the factors that influence the performance of the approach. For example, a facial recognition algorithm may perform poorly when image resolution is low or images are taken in low lighting. Or a speech-to-text system might not be used reliably to provide closed captions for online lectures because it fails to handle technical jargon.
   - The authors should discuss the computational efficiency of the proposed algorithms and how they scale with dataset size.
   - If applicable, the authors should discuss possible limitations of their approach to address problems of privacy and fairness.
   - While the authors might fear that complete honesty about limitations might be used by reviewers as grounds for rejection, a worse outcome might be that reviewers discover limitations that aren't acknowledged in the paper. The authors should use their best judgment and recognize that individual actions in favor of transparency play an important role in developing norms that preserve the integrity of the community. Reviewers will be specifically instructed to not penalize honesty concerning limitations.

3. **Theory assumptions and proofs**

   Question: For each theoretical result, does the paper provide the full set of assumptions and a complete (and correct) proof?

Answer: [Yes]

Justification: We provide the full set of assumptions for each theoretical result, with complete and correct proofs included in the appendix.

Guidelines:

- The answer NA means that the paper does not include theoretical results.
- All the theorems, formulas, and proofs in the paper should be numbered and cross-referenced.
- All assumptions should be clearly stated or referenced in the statement of any theorems.
- The proofs can either appear in the main paper or the supplemental material, but if they appear in the supplemental material, the authors are encouraged to provide a short proof sketch to provide intuition.
- Inversely, any informal proof provided in the core of the paper should be complemented by formal proofs provided in appendix or supplemental material.
- Theorems and Lemmas that the proof relies upon should be properly referenced.

4. **Experimental result reproducibility**

Question: Does the paper fully disclose all the information needed to reproduce the main experimental results of the paper to the extent that it affects the main claims and/or conclusions of the paper (regardless of whether the code and data are provided or not)?

Answer: [Yes]

Justification: We will release both our training and inference code, along with detailed instructions for constructing the dataset used in our experiments. While the actual dataset cannot be released due to constraints, all necessary steps and scripts will be provided to enable reproduction of the main results.

Guidelines:

- The answer NA means that the paper does not include experiments.
- If the paper includes experiments, a No answer to this question will not be perceived well by the reviewers: Making the paper reproducible is important, regardless of whether the code and data are provided or not.
- If the contribution is a dataset and/or model, the authors should describe the steps taken to make their results reproducible or verifiable.
- Depending on the contribution, reproducibility can be accomplished in various ways. For example, if the contribution is a novel architecture, describing the architecture fully might suffice, or if the contribution is a specific model and empirical evaluation, it may be necessary to either make it possible for others to replicate the model with the same dataset, or provide access to the model. In general. releasing code and data is often one good way to accomplish this, but reproducibility can also be provided via detailed instructions for how to replicate the results, access to a hosted model (e.g., in the case of a large language model), releasing of a model checkpoint, or other means that are appropriate to the research performed.
- While NeurIPS does not require releasing code, the conference does require all submissions to provide some reasonable avenue for reproducibility, which may depend on the nature of the contribution. For example
  (a) If the contribution is primarily a new algorithm, the paper should make it clear how to reproduce that algorithm.
  (b) If the contribution is primarily a new model architecture, the paper should describe the architecture clearly and fully.
  (c) If the contribution is a new model (e.g., a large language model), then there should either be a way to access this model for reproducing the results or a way to reproduce the model (e.g., with an open-source dataset or instructions for how to construct the dataset).
  (d) We recognize that reproducibility may be tricky in some cases, in which case authors are welcome to describe the particular way they provide for reproducibility. In the case of closed-source models, it may be that access to the model is limited in

some way (e.g., to registered users), but it should be possible for other researchers to have some path to reproducing or verifying the results.

5. **Open access to data and code**

   Question: Does the paper provide open access to the data and code, with sufficient instructions to faithfully reproduce the main experimental results, as described in supplemental material?

   Answer: [Yes]

   Justification: We will release our training and inference code on GitHub. The model and dataset will not be open-sourced, but we provide the detailed procedure for constructing the dataset. We partially release the dataset generation scripts, and the data preprocessing steps are described in the paper.

   Guidelines:

   - The answer NA means that paper does not include experiments requiring code.
   - Please see the NeurIPS code and data submission guidelines (`https://nips.cc/public/guides/CodeSubmissionPolicy`) for more details.
   - While we encourage the release of code and data, we understand that this might not be possible, so No is an acceptable answer. Papers cannot be rejected simply for not including code, unless this is central to the contribution (e.g., for a new open-source benchmark).
   - The instructions should contain the exact command and environment needed to run to reproduce the results. See the NeurIPS code and data submission guidelines (`https://nips.cc/public/guides/CodeSubmissionPolicy`) for more details.
   - The authors should provide instructions on data access and preparation, including how to access the raw data, preprocessed data, intermediate data, and generated data, etc.
   - The authors should provide scripts to reproduce all experimental results for the new proposed method and baselines. If only a subset of experiments are reproducible, they should state which ones are omitted from the script and why.
   - At submission time, to preserve anonymity, the authors should release anonymized versions (if applicable).
   - Providing as much information as possible in supplemental material (appended to the paper) is recommended, but including URLs to data and code is permitted.

6. **Experimental setting/details**

   Question: Does the paper specify all the training and test details (e.g., data splits, hyperparameters, how they were chosen, type of optimizer, etc.) necessary to understand the results?

   Answer: [Yes]

   Justification:We will include full training and test details in the supplementary material.These details are sufficient to understand and reproduce the experimental results.

   Guidelines:

   - The answer NA means that the paper does not include experiments.
   - The experimental setting should be presented in the core of the paper to a level of detail that is necessary to appreciate the results and make sense of them.
   - The full details can be provided either with the code, in appendix, or as supplemental material.

7. **Experiment statistical significance**

   Question: Does the paper report error bars suitably and correctly defined or other appropriate information about the statistical significance of the experiments?

   Answer: [Yes]

   Justification: The statistical significance of our experiments is evaluated by comparing the model's predictions with the gold-standard results generated by HSPICE simulations. We report root mean square error (R^2) as the primary metric to quantify the accuracy of our predictions. This provides a reliable and consistent measure of model performance.

Guidelines:

- The answer NA means that the paper does not include experiments.
- The authors should answer "Yes" if the results are accompanied by error bars, confidence intervals, or statistical significance tests, at least for the experiments that support the main claims of the paper.
- The factors of variability that the error bars are capturing should be clearly stated (for example, train/test split, initialization, random drawing of some parameter, or overall run with given experimental conditions).
- The method for calculating the error bars should be explained (closed form formula, call to a library function, bootstrap, etc.)
- The assumptions made should be given (e.g., Normally distributed errors).
- It should be clear whether the error bar is the standard deviation or the standard error of the mean.
- It is OK to report 1-sigma error bars, but one should state it. The authors should preferably report a 2-sigma error bar than state that they have a 96% CI, if the hypothesis of Normality of errors is not verified.
- For asymmetric distributions, the authors should be careful not to show in tables or figures symmetric error bars that would yield results that are out of range (e.g. negative error rates).
- If error bars are reported in tables or plots, The authors should explain in the text how they were calculated and reference the corresponding figures or tables in the text.

8. **Experiments compute resources**

   Question: For each experiment, does the paper provide sufficient information on the computer resources (type of compute workers, memory, time of execution) needed to reproduce the experiments?

   Answer: [Yes]

   Justification: All experiments were conducted on a single NVIDIA RTX 4090 GPU platform with 32 GB of memory. Training was performed on this platform, and the training time varied depending on the order of the system and the dataset size. Inference times are reported and compared in the main paper. The setup ensures that the experiments are reproducible on similar hardware.

   Guidelines:

   - The answer NA means that the paper does not include experiments.
   - The paper should indicate the type of compute workers CPU or GPU, internal cluster, or cloud provider, including relevant memory and storage.
   - The paper should provide the amount of compute required for each of the individual experimental runs as well as estimate the total compute.
   - The paper should disclose whether the full research project required more compute than the experiments reported in the paper (e.g., preliminary or failed experiments that didn't make it into the paper).

9. **Code of ethics**

   Question: Does the research conducted in the paper conform, in every respect, with the NeurIPS Code of Ethics `https://neurips.cc/public/EthicsGuidelines`?

   Answer: [Yes]

   Justification: We have reviewed the NeurIPS Code of Ethics and confirm that our work fully complies with it. Our research does not involve human data, privacy concerns, or potential for misuse. All results are reported transparently and responsibly.

   Guidelines:

   - The answer NA means that the authors have not reviewed the NeurIPS Code of Ethics.
   - If the authors answer No, they should explain the special circumstances that require a deviation from the Code of Ethics.
   - The authors should make sure to preserve anonymity (e.g., if there is a special consideration due to laws or regulations in their jurisdiction).

10. **Broader impacts**

    Question: Does the paper discuss both potential positive societal impacts and negative societal impacts of the work performed?

    Answer: [NA]

    Justification: This work is a technical study focused on physical modeling and simulation of high-order nonlinear systems to improve efficiency and accuracy in VLSI design. It has no direct societal applications and therefore does not discuss societal impacts. The method is primarily for engineering simulations with negligible risk of misuse or social issues like fairness or privacy.

    Guidelines:

    - The answer NA means that there is no societal impact of the work performed.
    - If the authors answer NA or No, they should explain why their work has no societal impact or why the paper does not address societal impact.
    - Examples of negative societal impacts include potential malicious or unintended uses (e.g., disinformation, generating fake profiles, surveillance), fairness considerations (e.g., deployment of technologies that could make decisions that unfairly impact specific groups), privacy considerations, and security considerations.
    - The conference expects that many papers will be foundational research and not tied to particular applications, let alone deployments. However, if there is a direct path to any negative applications, the authors should point it out. For example, it is legitimate to point out that an improvement in the quality of generative models could be used to generate deepfakes for disinformation. On the other hand, it is not needed to point out that a generic algorithm for optimizing neural networks could enable people to train models that generate Deepfakes faster.
    - The authors should consider possible harms that could arise when the technology is being used as intended and functioning correctly, harms that could arise when the technology is being used as intended but gives incorrect results, and harms following from (intentional or unintentional) misuse of the technology.
    - If there are negative societal impacts, the authors could also discuss possible mitigation strategies (e.g., gated release of models, providing defenses in addition to attacks, mechanisms for monitoring misuse, mechanisms to monitor how a system learns from feedback over time, improving the efficiency and accessibility of ML).

11. **Safeguards**

    Question: Does the paper describe safeguards that have been put in place for responsible release of data or models that have a high risk for misuse (e.g., pretrained language models, image generators, or scraped datasets)?

    Answer: [NA]

    Justification:This work is a technical simulation study and does not involve high-risk models or datasets that require special safeguards.

    Guidelines:

    - The answer NA means that the paper poses no such risks.
    - Released models that have a high risk for misuse or dual-use should be released with necessary safeguards to allow for controlled use of the model, for example by requiring that users adhere to usage guidelines or restrictions to access the model or implementing safety filters.
    - Datasets that have been scraped from the Internet could pose safety risks. The authors should describe how they avoided releasing unsafe images.
    - We recognize that providing effective safeguards is challenging, and many papers do not require this, but we encourage authors to take this into account and make a best faith effort.

12. **Licenses for existing assets**

    Question: Are the creators or original owners of assets (e.g., code, data, models), used in the paper, properly credited and are the license and terms of use explicitly mentioned and properly respected?

Answer: [NA]

Justification:We utilized Synopsys HSPICE (U-2023.03-SP2-2) under a valid institutional license for circuit simulations. Additionally, we employed open-source Python libraries with proper license acknowledgments provided in the supplemental materials.

Guidelines:

- The answer NA means that the paper does not use existing assets.
- The authors should cite the original paper that produced the code package or dataset.
- The authors should state which version of the asset is used and, if possible, include a URL.
- The name of the license (e.g., CC-BY 4.0) should be included for each asset.
- For scraped data from a particular source (e.g., website), the copyright and terms of service of that source should be provided.
- If assets are released, the license, copyright information, and terms of use in the package should be provided. For popular datasets, `paperswithcode.com/datasets` has curated licenses for some datasets. Their licensing guide can help determine the license of a dataset.
- For existing datasets that are re-packaged, both the original license and the license of the derived asset (if it has changed) should be provided.
- If this information is not available online, the authors are encouraged to reach out to the asset's creators.

13. **New assets**

Question: Are new assets introduced in the paper well documented and is the documentation provided alongside the assets?

Answer: [Yes]

Justification: We will release the relevant code and the dataset generation process alongside the paper. Detailed documentation, including usage instructions and experimental setups, will be provided in the supplementary material.

- The answer NA means that the paper does not release new assets.
- Researchers should communicate the details of the dataset/code/model as part of their submissions via structured templates. This includes details about training, license, limitations, etc.
- The paper should discuss whether and how consent was obtained from people whose asset is used.
- At submission time, remember to anonymize your assets (if applicable). You can either create an anonymized URL or include an anonymized zip file.

14. **Crowdsourcing and research with human subjects**

Question: For crowdsourcing experiments and research with human subjects, does the paper include the full text of instructions given to participants and screenshots, if applicable, as well as details about compensation (if any)?

Answer: [NA]

Justification: This work does not involve crowdsourcing or research with human subjects.

Guidelines:

- The answer NA means that the paper does not involve crowdsourcing nor research with human subjects.
- Including this information in the supplemental material is fine, but if the main contribution of the paper involves human subjects, then as much detail as possible should be included in the main paper.
- According to the NeurIPS Code of Ethics, workers involved in data collection, curation, or other labor should be paid at least the minimum wage in the country of the data collector.

15. **Institutional review board (IRB) approvals or equivalent for research with human subjects**

Question: Does the paper describe potential risks incurred by study participants, whether such risks were disclosed to the subjects, and whether Institutional Review Board (IRB) approvals (or an equivalent approval/review based on the requirements of your country or institution) were obtained?

Answer: [NA]

Justification: This work does not involve crowdsourcing or research with human subjects.

Guidelines:

- The answer NA means that the paper does not involve crowdsourcing nor research with human subjects.
- Depending on the country in which research is conducted, IRB approval (or equivalent) may be required for any human subjects research. If you obtained IRB approval, you should clearly state this in the paper.
- We recognize that the procedures for this may vary significantly between institutions and locations, and we expect authors to adhere to the NeurIPS Code of Ethics and the guidelines for their institution.
- For initial submissions, do not include any information that would break anonymity (if applicable), such as the institution conducting the review.

16. **Declaration of LLM usage**

Question: Does the paper describe the usage of LLMs if it is an important, original, or non-standard component of the core methods in this research? Note that if the LLM is used only for writing, editing, or formatting purposes and does not impact the core methodology, scientific rigorousness, or originality of the research, declaration is not required.

Answer: [NA]

Justification: The research uses Transformer architecture but does not involve large language models (LLMs) as core components.

- The answer NA means that the core method development in this research does not involve LLMs as any important, original, or non-standard components.
- Please refer to our LLM policy (https://neurips.cc/Conferences/2025/LLM) for what should or should not be described.